

Received 7 May 2023, accepted 29 May 2023, date of publication 31 May 2023, date of current version 23 June 2023.

Digital Object Identifier 10.1109/ACCESS.2023.3281672

RESEARCH ARTICLE

Disturbance Observer Based on Fixed Time Sliding Mode Control and Optimal State Observer for Three-Phase Three-Level T-Type Inverters

ANH TUAN DUONG^{1,2}, THANH LONG PHAM¹, VAN NAM GIAP¹, AND PHUONG VU¹

¹School of Electrical and Electronic Engineering, Hanoi University of Science and Technology, Hanoi 100000, Vietnam

²Faculty of Electrical Engineering, Hanoi University of Industry, Hanoi 100000, Vietnam

Corresponding authors: Van Nam Giap (nam.giapvan@hust.edu.vn) and Phuong Vu (phuong.vuhoang@hust.edu.vn)


This research is funded by Hanoi University of Science and Technology (HUST) under project number T2022-TD-001.

ABSTRACT This paper presents the advanced control method together with the disturbance rejection method with the aims to obtain the low of total harmonic distortion (THD). The expectation of the paper is that the output voltage is satisfied the requirements of the EN 62040 with the THD is less than 5%. Therefore, this paper proposes a new disturbance observer (DOB) without the requirement of the information of the first derivative disturbance for the three phase three level (TPTL) T-type inverter system. The proposed DOB is based on the information of the measurable states, which are used such an inversed model of T-type inverter to find the information of real disturbance. First, the DOB was designed based on the given measured and estimated states. However, to design the DOB, the state observer is required. Therefore, second, the state observer (SOB) was designed based on linear matrix inequality (LMI) to identify the optimal poles of the state-tracking error function. Third, the estimated states were used to construct the fixed time (FT) sliding mode control (SMC) to control the T-type inverter system. Fourth, the Lyapunov condition was used to verify the correction of the proposed method. The performance of the proposed control strategy is validated by simulations and experiments during steady-state, transients caused by load change, and unbalanced grid conditions. The estimated states precisely tracked the measured states. The output signals precisely converged to the predefined trajectories in a predefined time and the tracking errors are small. The obtained results showed that the proposed control method provided excellent steady-state and good performances with low THD in the line currents, zero steady-state error in the output voltage, and a very fast dynamic response.

INDEX TERMS Three-level T-type inverter, sliding mode control, state observer, linear matrix inequality, disturbance observer.

I. INTRODUCTION

In renewable energy applications, inverters can be categorized into two types: grid-tied and stand-alone inverters [1]. The grid-tied inverter converts the generated energy to feed directly to the grid. A stand-alone inverter draws electrical energy from the renewable energy source to supply the off-grid power system. A three-phase two-level inverter uses six bidirectional switches. The power supply should be a low (total harmonic distortion) THD and sine waves source. The multi-level inverter is an effective solution with applications

The associate editor coordinating the review of this manuscript and approving it for publication was Ching-Ming Lai .

for integrating renewable energy and AC drive. It solves the problem of harmonics of the output voltage, which is encountered by traditional two-level inverters for reducing the filter size at the same time protecting and reducing losses on the switches.

The multi-level inverters can be categorized as neutral point clamped (NPC) [2], [3], [4], cascaded H-bridge (CHB) [5], flying capacitor (FC) [6], T-type [7] and hybrid type [8], [9], [10]. Therefore, the T-type inverter has been utilizing more widely because of its advantage such as good output voltage quality, low switching losses, simple structure and requires only a DC power source [11]. The most important factor of the T-type inverters is how to obtain the optimal

configuration of the inverter with the bidirectional conduct. Furthermore, the against the high inversed voltage is difficult for the Insulated Gate Bipolar Transistors (IGBTs) and MOS-FETs. However, the reverse blocking IGBT (RB-IGBT) can easily obtain the expected goals of these mentioned problem and the power density together with the optimal size of the inverter dimension. Therefore, the RB-IGBT was selected for study in this paper.

The application of T-type inverter for the permanent magnet synchronous motor was discussed in [12]. The 5-level T-type inverter for six phase motor was discussed in [13]. The T-type inverter for aircraft was discussed in [14].

The PI control with the verifications of simulation and experiment were presented in [15]. A new, simplified space vector pulse-width modulation (SVPWM) for a TPTL T-type quasi-impedance source inverter was presented in [16]. A modified carrier level-shifted based control method for a PWM controlled TPTL T-type inverter was presented in [17]. In [18], Compensation of inverter nonlinearity of Three-level T-type inverters was presented. The feedforward decoupling control strategy and reactive power compensation was also presented in [19]. Paper [20] used deadbeat controller to obtain the finite time stability. In [21], a proportional-resonant (PR) control is used to damp the resonance in the LLCL filter. The authors in [22] proposed predictive observer based control method for single-phase T-type rectifier. The other studies devoted for three-level T-type rectifiers are based on EMI filter size minimization [23], improved modulation scheme for neutral-point potential balancing and circulating current suppression [24], and open-circuit [25] fault-tolerant control methods with neutral-point voltage oscillations suppression.

With the rapid developments of the power electronic systems the developments of hardware leads to the affect that the software also need to be grew up. The software is counted by the control algorithms. So such of that reason, in recent years, there are some advanced control methods have been developed instead of PI controller which is not easy to accomplish good performances under the perturbations. The perturbations in the power inverters can be listed as follows: The thermal changing of resistances, reluctance, capacitors are considered as the unwanted uncertain values. These values are usually counted as the uncertainties. Furthermore, the outside disturbances such as the loads of the converter systems are strongly unwanted terms Which should be cancelled by hardware or software. To easy in handle these inversed factors, the software implementation should be added into the control system. To obtain the good results for the inverter systems, the dead-beat in [26] and [27] were considered to give the good performances with high quantity output voltage and fast dynamic response. However, these controllers requested exact information about system parameters. In [28], a model predictive control (MPC) with load observer is proposed. Their controller guarantees a small steady-state error, and reduces the number of current sensors. But this scheme still gives a high THD level in the output voltage. A repetitive controller is

presented in [29]. With their algorithm, the voltage harmonic distortion is low, however the dynamic response is slow.

With the motivations of these listed papers [26], this paper presents a new SMC controller to make the three-level three-phase T-type inverter stable under some hard conditions such as: nonlinear or linear load, balanced or unbalanced load, parameters system is faulty, time-varying disturbance.

Furthermore, this paper is designed a new DOB for T-type inverter without the requirement of the first derivative disturbance such as in the previous papers [30], [31], [32]. Furthermore, the proposed DOB in this paper is not request the format of the disturbance such as in previous paper [33], [34], [35]. The contributions to reject these requirements of first derivative and fixed format requirements are important factor in the unknown input observer area. Therefore, disturbance with any frequency are all rejected theoretically. Taking advantage of our proposed method in [36], a DOB for T-type inverter is successfully designed for estimating the complicated variations of parameters and the load compensation. The stability of the proposed DOB is finite time. Basically, the DOB of this paper requires the information of the measured and estimated states. Therefore, the state observer is requested. To simplify the design and present clearly the new contribution, the state observer in this paper is optimally designed based on the extended state observer format. The gains of the state observer were obtained by using the vertical LMI such as in [37]. The discussion of the extended state observer can be found in [38]. The fault tolerance methods for T-type inverter can be found in [39], [40], and [41].

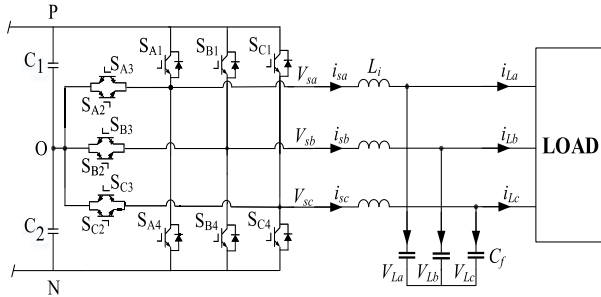
The proposed controller uses both inner and outer control loops with the same structure. Each control loop uses the FTSMC controller [33], combined with SOB and DOB, the contributions of this paper are listed as follows:

1. The system states of the TPTL T-type inverter such as the output currents and load voltages can be precisely estimated by the support of the LMI method with vertical spaces. These estimated states were used to construct SMC for both control of voltage and current loops
2. The FTSMC was designed for controlling the TPTL T-type inverter with a simple and effective structure. In SMC design, the estimated state and reference input are used to build the surface. Furthermore, the proposed DOB is given based on the information of the measured and estimated states.
3. To show the correction and effectiveness of proposed controller on the TPTL T-type inverter, the proof was theoretically provided together with the simulation by using MATLAB software and experimental study.

The using of disturbance observer with the aim of softening the chattering factor, which coursed from the gains of the SMC. To DO is used to estimate the high and low frequency disturbance observer. After using the DO, the SMC can be

TABLE 1. Switching state for phase B.

State	V_{out}	S_{B1}	S_{B2}	S_{B3}	S_{B4}
P	$V_{DC}/2$	ON	ON	OFF	OFF
O	0	OFF	ON	ON	OFF
N	$-V_{DC}/2$	OFF	OFF	ON	ON


FIGURE 1. TPTL T-type inverter.

design with small switching gains, which leads the chattering is significant reduced.

The next sections of the paper consists of the section II, the operation principle of a three-phase three-level T-type inverter is presented. Section III presents mathematical model of a three-phase three-level T-type inverter and preliminary mathematics. The control methods for the T-type inverter system is give in section IV. Section V is given to show the simulation and experimental results, respectively. Finally, section VI presents the conclusion of this study.

II. OPERATION PRINCIPLE OF A TPTL T-TYPE INVERTER

The TPTL T-type inverter shown in Fig. 1, each phase consists of three power switches (2 IGBTs and 1 RB-IGBT) [42]. Switching on and off power switches in appropriate ways will generate a three-phase output voltage at three levels: $+V_{DC}/2$, 0, $-V_{DC}/2$. Table 1 illustrates the switching state according to phase B output voltages.

III. MATHEMATICAL MODEL OF A THREE-PHASE THREE LEVEL T-TYPE INVERTER AND PRELIMINARY MATHEMATICS

This section is used to show the mathematical model of a three-phase three-level T-type inverter and mathematical operations on LMI, FTSMC, DOB and SOB.

A. MATHEMATICAL MODELING OF THE THREE-PHASE THREE-LEVEL T-TYPE INVERTER

By applying the Kirchhoff's law for circuit at the point where the filter is connected yields

$$C_f \frac{dv_{Lk}}{dt} = i_{sk} - i_{Lk} \quad (1)$$

where C_f is the capacitance of the LC filter, the subscript $k = a, b, c$ illustrates the different phases of the system, v_{Lk} is the load voltage, which is the desired control objective, i_{sk} is current at the output-side of the T-type inverter, and i_{Lk} is the load current.

Transferring to synchronous d - q reference frame using Park transformation:

$$\begin{cases} C_f \frac{dv_{Ld}}{dt} = i_{sd} - i_{Ld} + \omega \cdot C_f \cdot v_{Lq} \\ C_f \frac{dv_{Lq}}{dt} = i_{sq} - i_{Lq} - \omega \cdot C_f \cdot v_{Ld} \end{cases} \quad (2)$$

where $v_{Ld} - v_{Lq}$, $i_{sd} - i_{sq}$, $i_{Ld} - i_{Lq}$ are load voltage, inverter current and load current in d and q axes, respectively. ω is the changing speed of the voltage.

Transformation in matrix form, leading to

$$\begin{bmatrix} \dot{v}_{Ld} \\ \dot{v}_{Lq} \end{bmatrix} = \begin{bmatrix} 0 & \omega \\ -\omega & 0 \end{bmatrix} \cdot \begin{bmatrix} v_{Ld} \\ v_{Lq} \end{bmatrix} + \begin{bmatrix} \frac{1}{C_f} & 0 \\ 0 & \frac{1}{C_f} \end{bmatrix} \cdot \begin{bmatrix} i_{sd} - i_{Ld} \\ i_{sq} - i_{Lq} \end{bmatrix} \quad (3)$$

To facilitate the process of calculating and designing the controller in the next sections, referring

$$X_1 = \begin{bmatrix} v_{Ld} \\ v_{Lq} \end{bmatrix}, \quad A_1 = \begin{bmatrix} 0 & \omega \\ -\omega & 0 \end{bmatrix}, \quad B_1 = \begin{bmatrix} \frac{1}{C_f} & 0 \\ 0 & \frac{1}{C_f} \end{bmatrix}$$

$$\text{and } u_1 = \begin{bmatrix} i_{sd} - i_{Ld} \\ i_{sq} - i_{Lq} \end{bmatrix}.$$

By applying Kirchhoff's voltage law at the outside of the circuit, we have

$$L_f \frac{di_{sk}}{dt} = v_{sk} - v_{Lk} \quad (4)$$

where L_f is the inductance of the LC filter, the subscript $k = a, b, c$ illustrates the different phases of the system, v_{Lk} is the load voltage, v_{sk} is the output voltage of the T-type inverter, i_{sk} is current at the output-side of the T-type inverter, transferring to synchronous $d - q$ reference frame using Park transformation:

$$\begin{cases} L_f \frac{di_{sd}}{dt} = v_{sd} - v_{Ld} + \omega L_f \cdot i_{sq} \\ L_f \frac{di_{sq}}{dt} = v_{sq} - v_{Lq} - \omega L_f \cdot i_{sd} \end{cases} \quad (5)$$

where $v_{Ld} - v_{Lq}$, $i_{sd} - i_{sq}$, $i_{Ld} - i_{Lq}$ are load voltage, inverter current and voltage in dq coordinatng system, respectively.

Transformation in matrix form, leads to

$$\begin{bmatrix} \dot{i}_{sd} \\ \dot{i}_{sq} \end{bmatrix} = \begin{bmatrix} 0 & \omega \\ -\omega & 0 \end{bmatrix} \cdot \begin{bmatrix} i_{sd} \\ i_{sq} \end{bmatrix} + \begin{bmatrix} \frac{1}{L_f} & 0 \\ 0 & \frac{1}{L_f} \end{bmatrix} \cdot \begin{bmatrix} v_{sd} - v_{Ld} \\ v_{sq} - v_{Lq} \end{bmatrix} \quad (6)$$

Similar to the above, to facilitate the process of calculating and designing the controller in the next sections, referring

$$X_2 = \begin{bmatrix} i_{sd} \\ i_{sq} \end{bmatrix}, \quad A_2 = \begin{bmatrix} 0 & \omega \\ -\omega & 0 \end{bmatrix}, \quad B_2 = \begin{bmatrix} \frac{1}{L_f} & 0 \\ 0 & \frac{1}{L_f} \end{bmatrix},$$

and $u_2 = \begin{bmatrix} v_{sd} - v_{Ld} \\ v_{sq} - v_{Lq} \end{bmatrix}$.

Remark 1: The separated equations of overall model such as in the equations (3) and (6) with the aim of softening the calculation in the control design.

B. PRELIMINARY MATHEMATICS

This section is used to describe the mathematical operations of FTSMC, LMI and exponential convergence DOB.

1) FIXED-TIME SLIDING MODE CONTROL

Consider the system

$$\dot{x} = f(x, t) \tag{7}$$

where $x(0) = x_0 \cdot x \in R^n$, and $f(x) \in R^n$.

Definition 1: FT stability [43].

System (7) is called FT stable if the settling time is globally bounded.

Lemma 1: Consider the equation [43]

$$\dot{s} = -\alpha_1 sig^{a_1}_{b_1}(s) - \alpha_2 sig^{a_2}_{b_2}(s) \tag{8}$$

where $a_1 > b_1, a_2 < b_2, \alpha_1$ and α_2 , are positive values, s is the scalar variable of time, which some time used for the sliding mode surface and $sig(s) = |s| sign(s)$ Therefore, the settling time is bounded as follows:

$$T < T_{max} = \frac{1}{\alpha_1} \frac{b_1}{a_1 - b_1} + \frac{1}{\alpha_2} \frac{b_2}{a_2 - b_2} \tag{9}$$

where T_{max} is the maximum value of the settling time. T is the real settling time of the reaching law in Eq. (8).

Proof: The Lyapunov candidate can be chosen by

$$V(s) = \frac{1}{2} s^2 \tag{10}$$

Taking derivative for Eq. (10) yields

$$\begin{aligned} \dot{V}(s) &= s\dot{s} \\ &= s(-\alpha_1 sig^{a_1}_{b_1}(s) - \alpha_2 sig^{a_2}_{b_2}(s)) \\ &= -\alpha_1 \delta^{2\frac{a_1+b_1}{2b_1}} - \alpha_2 \delta^{2\frac{a_2+b_2}{2b_2}} \\ &= -\alpha_1 V(s)^{\frac{a_1+b_1}{2b_1}} - \alpha_2 V(s)^{\frac{a_2+b_2}{2b_2}} \\ &= \left[-\alpha_1 V(s)^{\frac{a_1+b_1}{2b_1} - \frac{a_2+b_2}{2b_2}} - \alpha_2 \right] V(s)^{\frac{a_2+b_2}{2b_2}} \\ &\leq 0 \end{aligned} \tag{11}$$

Because $\dot{V}(s) \leq 0$ system (7) is globally bounded. $V(s) = 0$ is a simple case. $V(\delta) \neq 0$ leads to

$$\frac{1}{V(s)^{\frac{a_2+b_2}{2b_2}}} \frac{dV(s)}{dt} = -\alpha_1 V(s)^{\frac{a_1+b_1}{2b_1} - \frac{a_2+b_2}{2b_2}} - \alpha_2 \tag{12}$$

or

$$\begin{aligned} &\frac{1}{V(s)^{\frac{a_2+b_2}{2b_2}}} \frac{dV(s)}{dt} \\ &= -\alpha_1 V(s)^{\frac{a_1+b_1}{2b_1} - \frac{a_2+b_2}{2b_2}} - \alpha_2 \\ &\quad \times \frac{1}{\alpha_1 V(s)^{\frac{b_2 a_1 - b_1 a_2}{2b_1 b_2}} + \alpha_2} \frac{dV(s)}{dt} = \frac{b_2 - a_2}{b_2} \end{aligned} \tag{13}$$

Integrating (14) over the time from zero to T yields

$$\int_0^T \frac{V(\delta)^{\frac{b_2-a_2}{2b_2}}}{\alpha_1 V(\delta)^{\frac{b_2-a_2}{2b_2} \left[\frac{(b_2 a_1 - b_1 a_2)}{b_1 (b_2 - a_2)} + 1 \right]} + \alpha_2} = \frac{b_2 - a_2}{2b_2} T \tag{14}$$

or

$$T < \frac{1}{\frac{b_2-a_2}{2b_2}} \int_0^1 \frac{d\zeta}{\alpha_2} + \frac{1}{\frac{b_2-a_2}{2b_2}} \int_1^\infty \frac{V(\delta)^{\frac{b_2-a_2}{2b_2}}}{\alpha_1 V(\delta)^{\frac{(b_2 a_1 - b_1 a_2)}{2b_1 b_2} + \frac{b_2-a_2}{2b_2}}} \tag{15}$$

$$= \frac{1}{\alpha_2} \frac{b_2}{b_2 - a_2} + \frac{1}{\alpha_1} \frac{b_2}{b_2 - a_2} \frac{b_1(b_2 - a_2)}{(b_2 a_1 - b_1 a_2)} \tag{16}$$

or

$$T_{max} = \frac{1}{\alpha_2} \frac{b_2}{b_2 - a_2} + \frac{1}{\alpha_1} \frac{b_1}{(a_1 - b_1)} \tag{17}$$

This completes the proof of lemma 1.

Remark 2: To help the reader easy to understand the main idea of the presented control method, the proof of lemma 1 is given from Eq. (10) to Eq. (17). For such a scalar function of time in format of Eq. (8), the variable of that equation can go back to the equivalent point after a predefined time such as in Eq. (17).

2) LINEAR MATRIX INEQUALITY

Definition 2: LMI in [34]. Consider the system

$$\dot{x}(t) = Ax(t) \tag{18}$$

where x is state and A is an approximated matrix of x . System (18) is called LMI stable if there exists a positive matrix P that satisfies

$$A^T P + PA < 0 \tag{19}$$

This paper used the vertical area to find the eigenvalues of the system state errors. The vertical area is referred to as

$$V = \{z \in C : f_v(z) < 0\} \tag{20}$$

where

$$f_v(z) = a + zb + \bar{z}b \tag{21}$$

The V area can be shown as follows:

Lemma 2: For eigenvalues of (18) located in the V area, the eigenvalues of A satisfy $-b < eig(A) < -a$ which can be represented as follows:

$$\begin{cases} A^T P + PA + 2aP < 0 \\ A^T P + PA + 2bP > 0 \end{cases} \tag{22}$$

Proof: The Lyapunov candidates for system (18) are selected as follows:

$$V(x) = x^T P x \tag{23}$$

Taking the derivative of both sides of Eq. (23) yields

$$\begin{aligned} \dot{V}(x) &= \dot{x}^T P x + x^T P \dot{x} \\ &= x^T A^T P x + x^T P A x \\ &= x^T (A^T P + P A) x \end{aligned} \tag{24}$$

$$\dot{V}(x) < 0 \quad \text{and} \quad -b < \text{eig}(A) < -a \tag{25}$$

$$\text{if } \begin{cases} (A + Ia)^T P + P(A + Ia) < 0 \\ (A + Ib)^T P + P(A + Ib) > 0 \end{cases} \tag{26}$$

or

$$\begin{cases} A^T P + P A + 2aP < 0 \\ A^T P + P A + 2bP > 0 \end{cases} \tag{27}$$

This completes the proof of lemma 2.

Remark 3: Lemma 2 is used to define the observer gains of Eq. (42), where the states observer gains are placed in the LMI region.

3) STATE OBSERVER

Definition 3: DO-based state observer error.

To show the DO for this state observer error-based system, the state-space equation is as follows:

$$\begin{cases} \dot{X} = AX + Bu + Dd \\ y = CX \end{cases} \tag{28}$$

where $X \in R^{m \times n}$ is the state vector, $Y \in R^{k \times n}$ is the system output vector, $A \in R^{m \times m}$, $B \in R^{m \times p}$, $C \in R^{k \times m}$ and $D \in R^{m \times q}$ are the approximated matrices of states, control input, and perturbations vectors, respectively, and $u \in R^{p \times m}$ is the control input vector. System (28) can work if the disturbance and uncertainty are bounded assumed as $|d| < \kappa$, where κ is positively defined. The estimated system of the (28) can be designed as follows:

$$\begin{cases} \dot{\hat{X}} = A\hat{X} + Bu + D\hat{d} - LC(X - \hat{X}) \\ \hat{y} = C\hat{X} \end{cases} \tag{29}$$

where L is the gain of the state observer, which need to be defined by the designer. \hat{d} is the estimated disturbance. First, consider the case of no disturbance effects on the system (28). The state error can be represented as

$$\dot{e}_X = (A + LC)e_X \tag{30}$$

where $e_X = X - \hat{X}$. By applying the LMI toolbox, the observer gain L is found with

$$\begin{cases} (A + LC)^T P + P(A + LC) + 2aP < 0 \\ (A + LC)^T P + P(A + LC) + 2bP > 0 \end{cases} \tag{31}$$

where P, a, b are positively defined. These a and b are the values of the gap of the LMI condition. The eigenvalues of the Eq. (30) will optimally found by using the MALAB code function with the command of LMI solver.

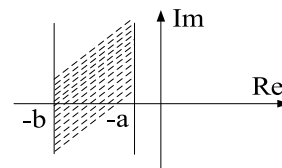


FIGURE 2. Vertical LMI region.

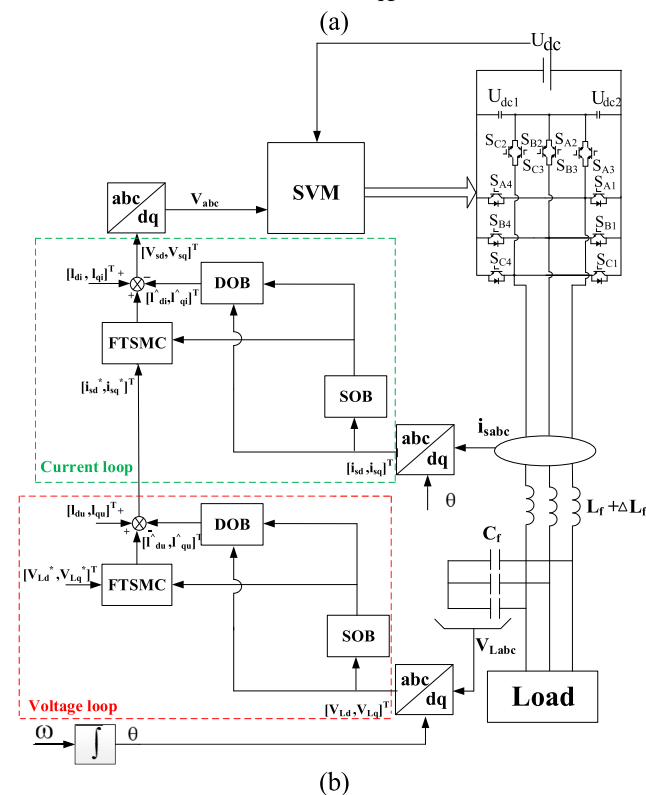
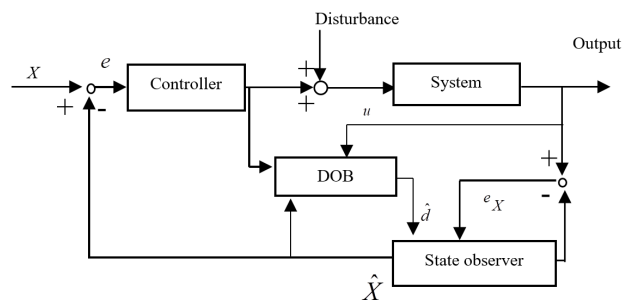


FIGURE 3. Diagram of the proposed algorithms for three-phase three-level T-type inverter.

4) DISTURBANCE OBSERVER

Herein, the concept of DOB in [36] is reused to design the DO for the inverter system. The disturbance also needs to be estimated exactly, starting from the system of equations (28) and (29) lead to:

$$\begin{cases} \dot{X} - Bu - Dd = AX \\ \dot{\hat{X}} = A\hat{X} + Bu + D\hat{d} - LC(X - \hat{X}) \end{cases} \tag{32}$$

TABLE 2. Simulation parameters.

Parameters	Value
DC bus voltage	600V
Output voltage	380V/50Hz
Switching frequency	10kHz
LC filter	1mH/20μF
DC-link capacitor	940μF
Load	9.68Ω

TABLE 3. Control parameters.

Parameters	Value
Voltage loop	$L=-2500, \kappa=\rho_1=\rho_2=0.0005,$ $\lambda=3000, c_1=4, c_2=5, d_1=5,$ $d_2=4$
Current loop	$L=-10000, \kappa=\rho_1=\rho_2=0.0005,$ $\lambda=10000, c_1=4, c_2=6, d_1=6,$ $d_2=4$

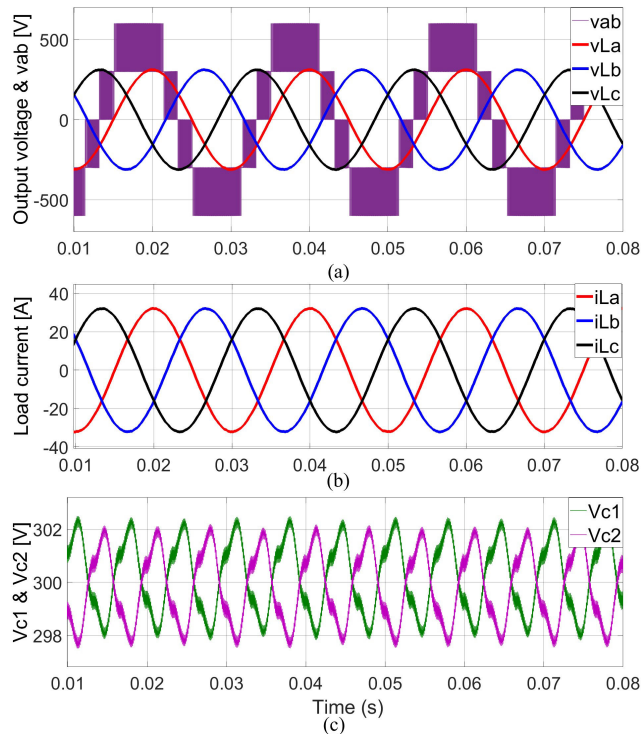


FIGURE 4. Simulated steady-state responses of $(v_{La}, v_{Lb}, v_{Lc}), v_{ab}, (i_{La}, i_{Lb}, i_{Lc}),$ and (V_{c1}, V_{c2}) under linear load.

Subtracting the two sides of the equations in the system of equations (32) yields

$$\dot{X} - \dot{\hat{X}} - Bu - Dd$$

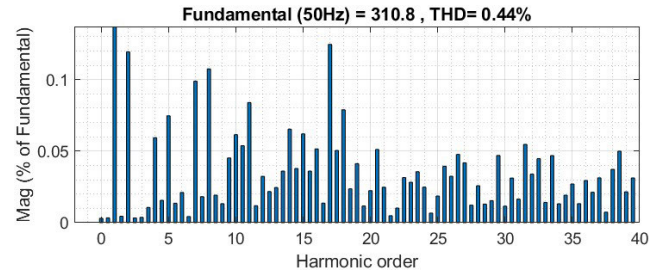


FIGURE 5. Three-phase load voltage FFT analysis under linear load.

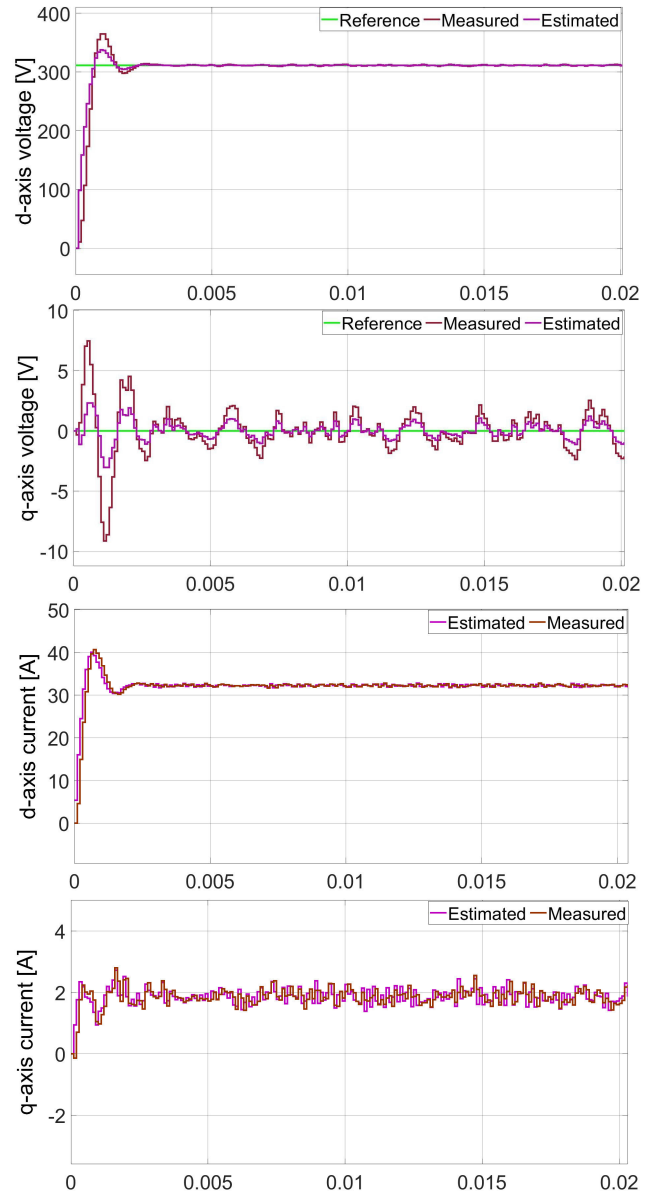


FIGURE 6. Reference, estimated and measured d-axis and q-axis voltage and current under linear load.

$$= AX - A\hat{X} - Bu - D\hat{d} + LC(X - \hat{X}) \quad (33)$$

$$\Rightarrow (\dot{X} - \dot{\hat{X}}) - Dd + D\hat{d} = (A + LC)(X - \hat{X}) \quad (34)$$

$$\Rightarrow (\dot{X} - \dot{\hat{X}}) - Dd = (A + LC)(X - \hat{X}) \quad (35)$$

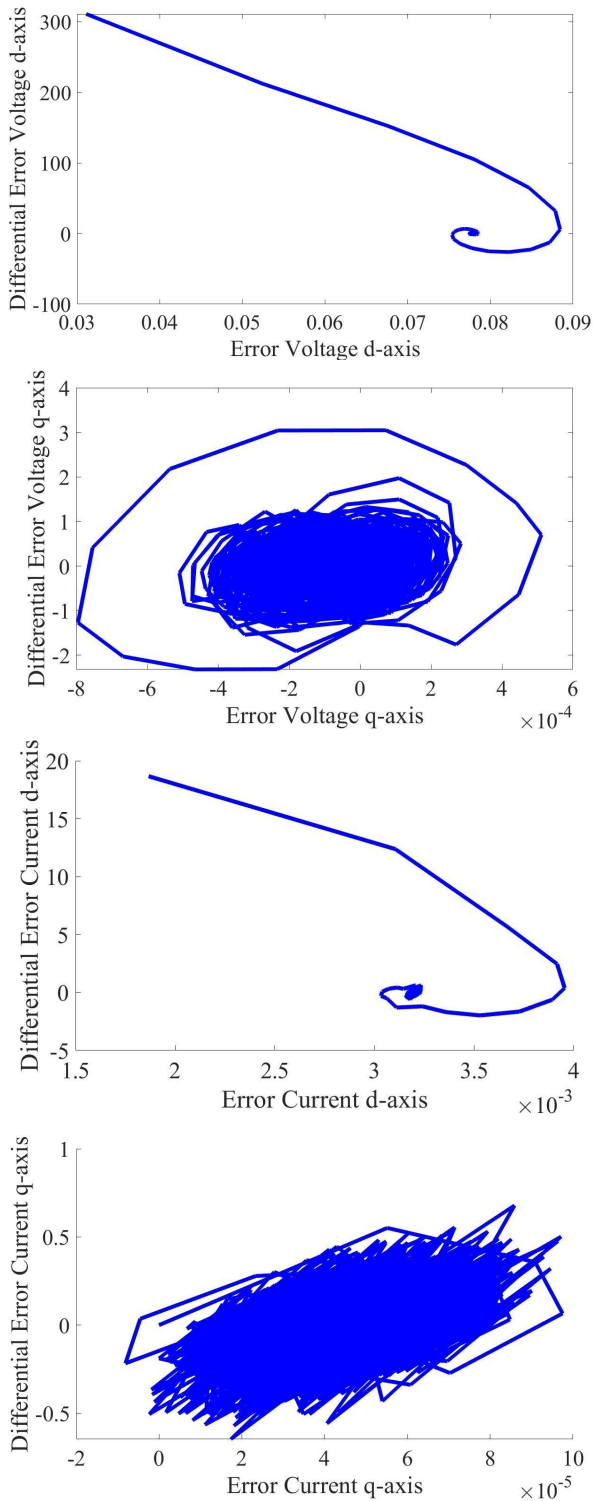


FIGURE 7. Error and differential error d-axis and q-axis voltage and current.

But $\dot{e}_X = \dot{X} - \dot{\hat{X}} \rightarrow 0$ and D is a square matrix, so we have:

$$\tilde{d} = -D^{-1} (A + LC) (X - \hat{X}) \quad (36)$$

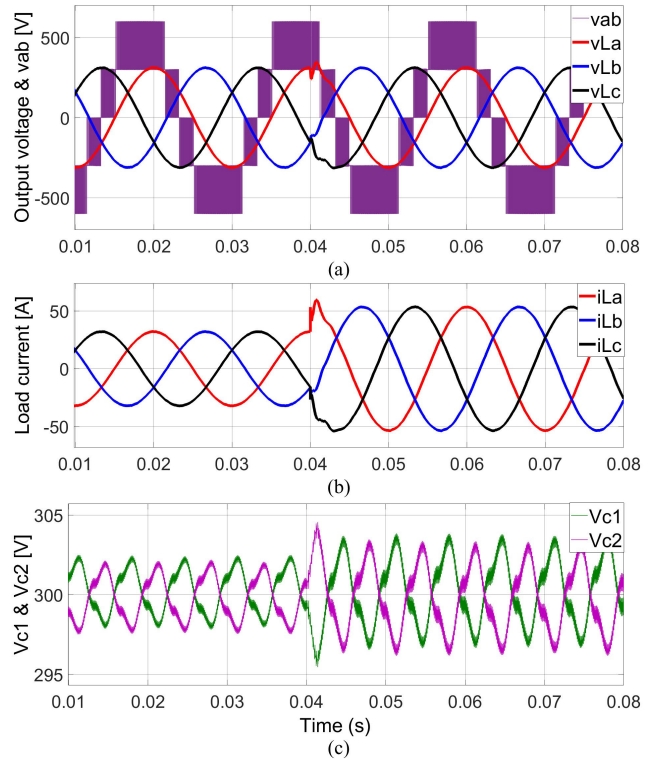


FIGURE 8. Simulated steady-state responses of (v_{La}, v_{Lb}, v_{Lc}) , v_{ab} , (i_{La}, i_{Lb}, i_{Lc}) , and (V_{c1}, V_{c2}) under load changes.

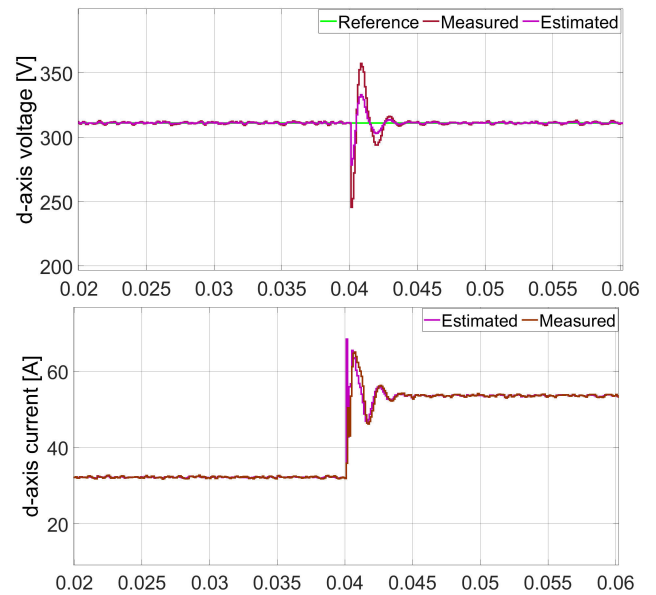


FIGURE 9. Reference, estimated and measured d-axis voltage and current under load changes.

where $\tilde{d} = d - \hat{d}$ leads to

$$\tilde{d} = -D^{-1} [(A + LC) (X - \hat{X}) - D\hat{d}] \quad (37)$$

Like the SOB stage, to estimate the noise accurately, $\tilde{d} = d - \hat{d} \rightarrow 0$. To satisfy this, we choose the following convergence

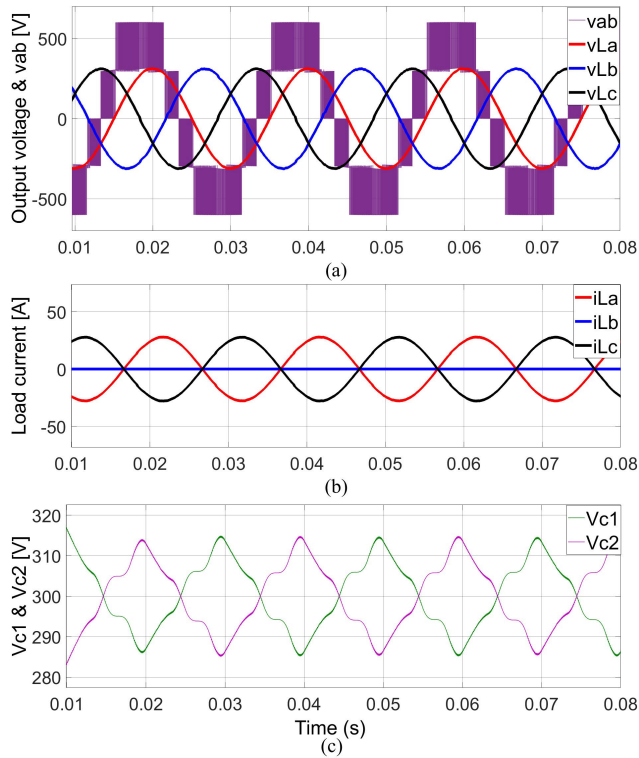


FIGURE 10. Simulated steady-state responses of (v_{La} , v_{Lb} , v_{Lc}), v_{ab} , (i_{La} , i_{Lb} , i_{Lc}), and (V_{c1} , V_{c2}) under unbalanced load.

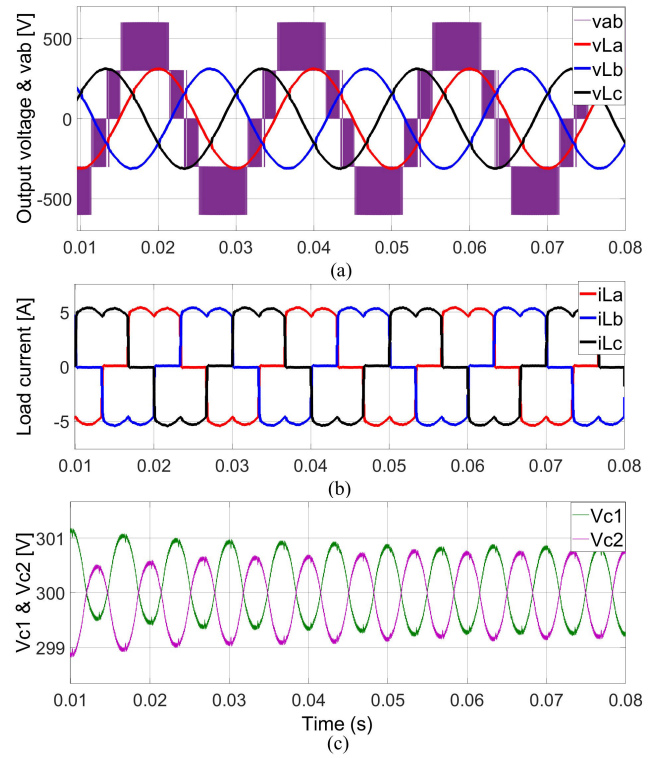


FIGURE 12. Simulated steady-state responses of (v_{La} , v_{Lb} , v_{Lc}), v_{ab} , (i_{La} , i_{Lb} , i_{Lc}), and (V_{c1} , V_{c2}) under nonlinear load.

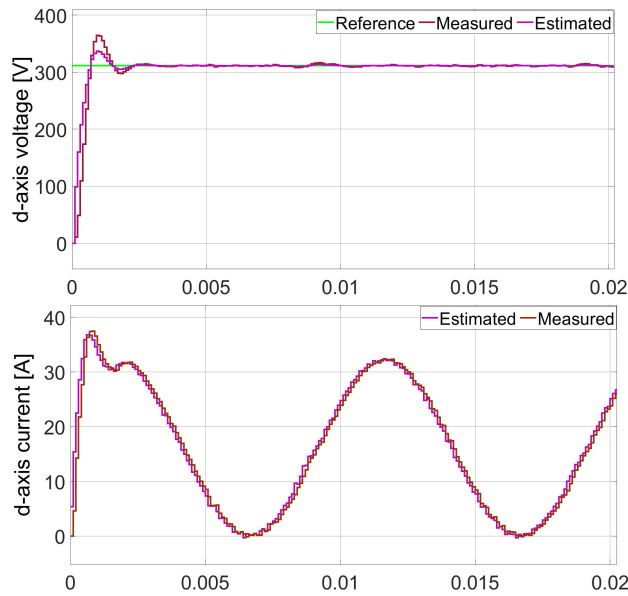


FIGURE 11. Reference, estimated and measured d-axis voltage and current under unbalanced load.

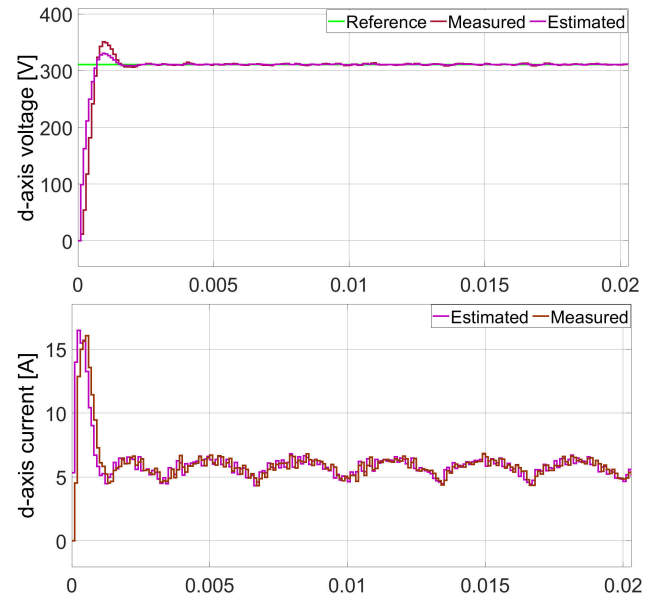


FIGURE 13. Reference, estimated and measured d-axis voltage and current under nonlinear load.

law:

$$\tilde{d} = -\kappa \int \tilde{d} \quad (38)$$

where: κ is a positive number.

$$\Rightarrow \hat{d} = d + \kappa \int \tilde{d} \quad (39)$$

The stability of the DOB has also been demonstrated in detail in [36]

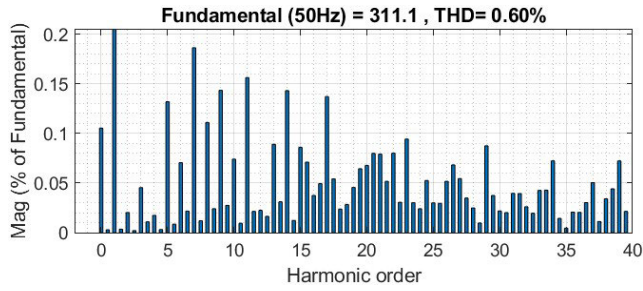


FIGURE 14. Three-phase load voltage FFT analysis under unbalanced load.

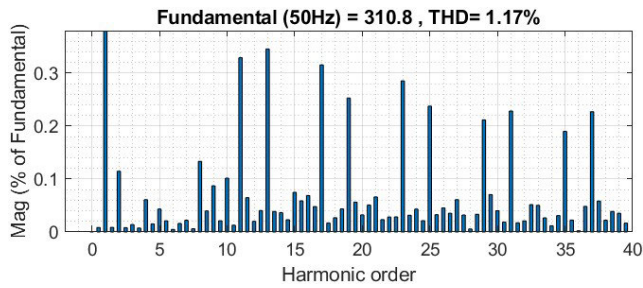


FIGURE 15. Three-phase load voltage FFT analysis under nonlinear load.

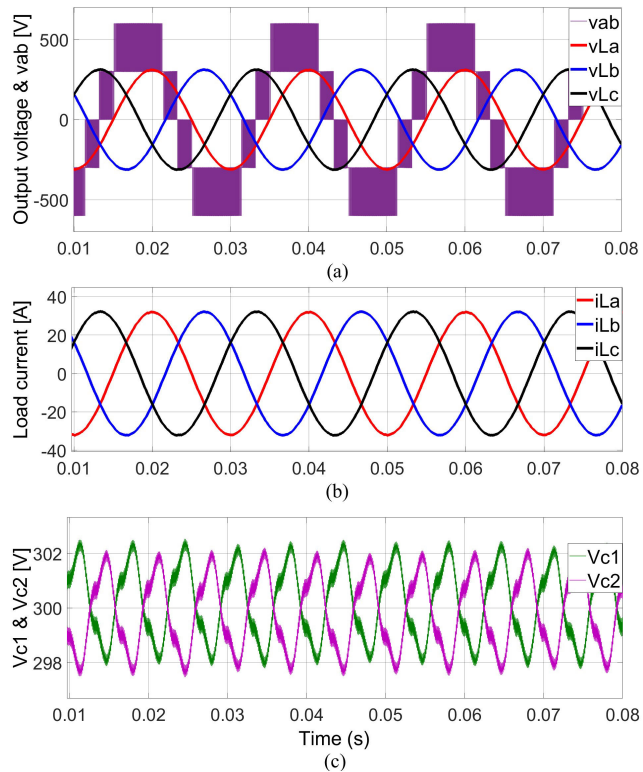


FIGURE 16. Simulated steady-state responses of $(v_{La}, v_{Lb}, v_{Lc}), v_{ab}, (i_{La}, i_{Lb}, i_{Lc}),$ and (V_{c1}, V_{c2}) when the exact system parameters are unknown.

Remark 4: The information of d in Eq. (39) can be obtained by using Eq. (36) with the subtraction of the estimated disturbance.

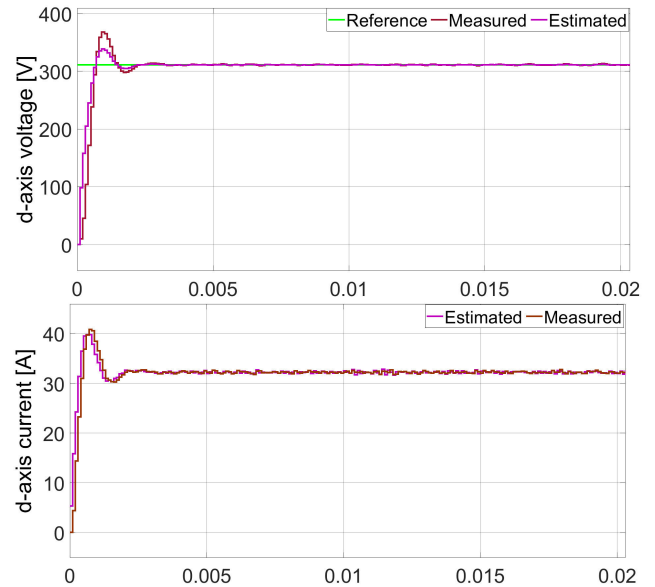


FIGURE 17. Reference, estimated and measured d-axis and q-axis voltage and current when the exact system parameters are unknown (Design: $L_a = L_b = L_c = L,$ reality: $L_a = 1.1 * L, L_b = L, L_c = 0.9 * L$).

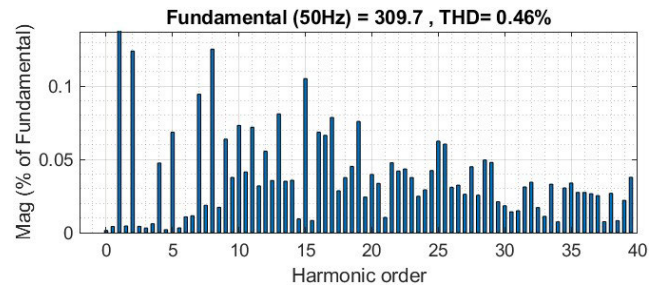


FIGURE 18. Three-phase load voltage FFT analysis when the system parameters are not known exactly.

IV. PROPOSED APPROACH

This section shows the application of the proposed controller for the three-phase three-level T -type inverter. First, state and disturbance observers are designed for the T -type inverter. Then, the FTSMC is designed with full states feedback for controlling the system.

Remark 5: This paper uses a cascade control structure consisting of two control loops: the inner loop is a current control system, and the outer loop is a voltage control system. Both loops will be designed with the same architecture. In this section, the X values will represent X_1 and X_2 , the A values will represent A_1 and A_2 , the B values will represent B_1 and B_2 , the d values will represent d_1 and d_2 , and the u values will represent u_1 and u_2 . With $A_1, A_2, B_1, B_2, d_1, d_2, u_1,$ and u_2 are mentioned in section III.

A. DISTURBANCE OBSERVER FOR TPTL T-TYPE INVERTER

The TPTL T -type inverter with fully disturbance is rewritten by

$$\begin{cases} \dot{X} = (A + \Delta A) X + (B + \Delta B)u + Dd \\ y = CX \end{cases} \quad (40)$$

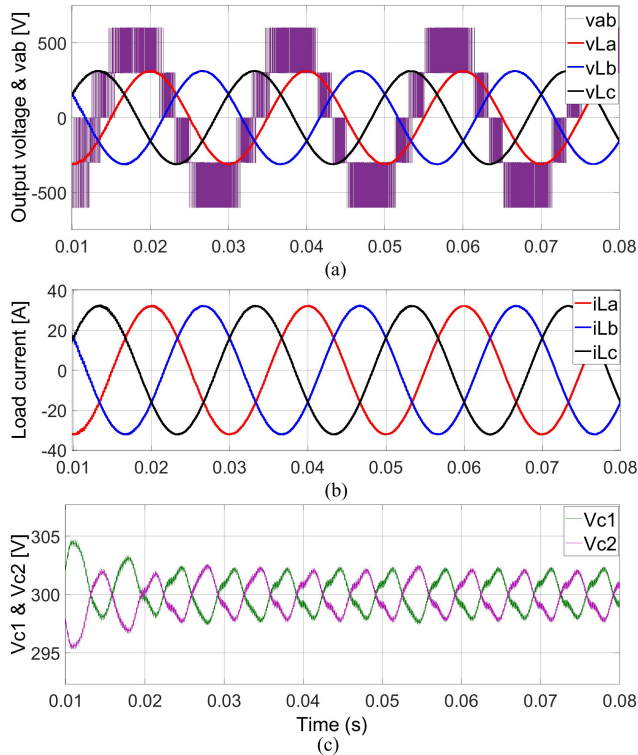


FIGURE 19. Simulated steady-state responses of $(v_{La}, v_{Lb}, v_{Lc}), v_{ab}, (i_{La}, i_{Lb}, i_{Lc}),$ and (V_{c1}, V_{c2}) under linear load and PI controller.

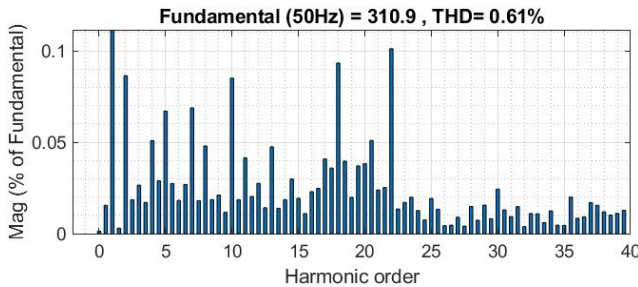


FIGURE 20. Three-phase load voltage FFT analysis under linear load and PI controller.

To easily obtain the information of the perturbations, these terms should be grouped as one term $\Delta A \cdot X + \Delta B \cdot u + Dd = E \cdot l$

System (40) can be written as follows:

$$\begin{cases} \dot{X} = A.X + B.u + E.l \\ y = CX \end{cases} \quad (41)$$

Remark 6: Matrix E should be identity defined. The variations of these parameters are unknown.

$$\begin{cases} \dot{\hat{X}} = A\hat{X} + Bu + E\hat{l} - LC(X - \hat{X}) \\ \hat{y} = C\hat{X} \\ \hat{l} = l + \kappa \int \tilde{l} \end{cases} \quad (42)$$

Remark 7: The estimated disturbance was used to compensate the disturbance of the three-phase three-level T -type inverter via the control input channel.

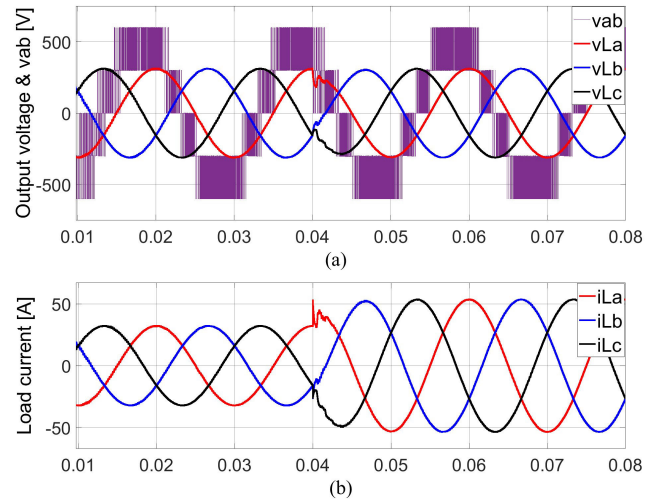


FIGURE 21. Simulated steady-state responses of $(v_{La}, v_{Lb}, v_{Lc}), v_{ab}, (i_{La}, i_{Lb}, i_{Lc})$ under load changed and PI controller.

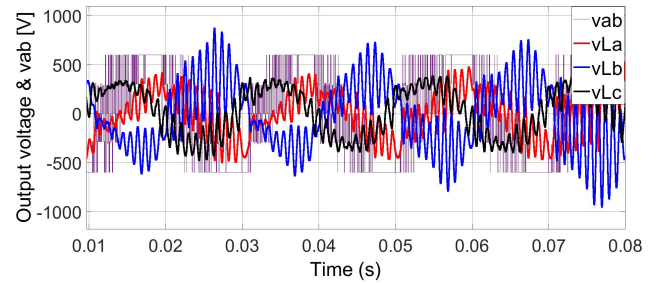


FIGURE 22. Simulated steady-state responses of $(v_{La}, v_{Lb}, v_{Lc}), v_{ab}$ under unbalanced load and PI controller.

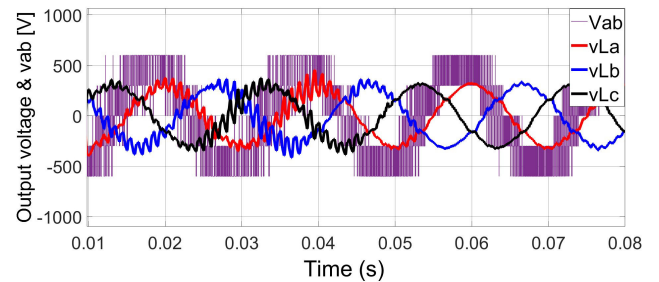


FIGURE 23. Simulated steady-state responses of $(v_{La}, v_{Lb}, v_{Lc}), v_{ab}$ under nonlinear load and PI controller.

B. STATE OBSERVER FOR THREE-PHASE THREE-LEVEL T-TYPE INVERTER

By combining of system (41) and (42), the tracking error equation can be modeled as follows:

$$\begin{cases} \dot{X} - \dot{\hat{X}} = A(X - \hat{X}) + E(l - \hat{l}) + LC(X - \hat{X}) \\ y - \hat{y} = C(X - \hat{X}) \end{cases} \quad (43)$$

$$\Rightarrow \dot{e}_X = Ae_X + LCe_X \quad (44)$$

$$\Rightarrow \dot{e}_X = (A + LC)e_X \quad (45)$$

where $e_X = X - \hat{X}$

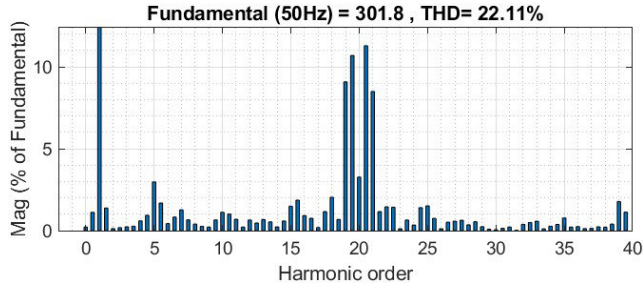


FIGURE 24. Three-phase load voltage FFT analysis under nonlinear load and PI controller.

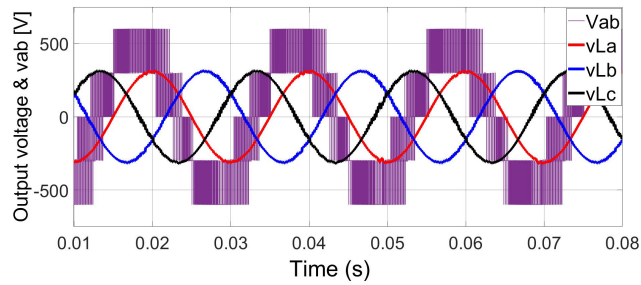


FIGURE 25. Simulated steady-state responses of (v_{La} , v_{Lb} , v_{Lc}), v_{ab} under PI controller when the exact system parameters are unknown.

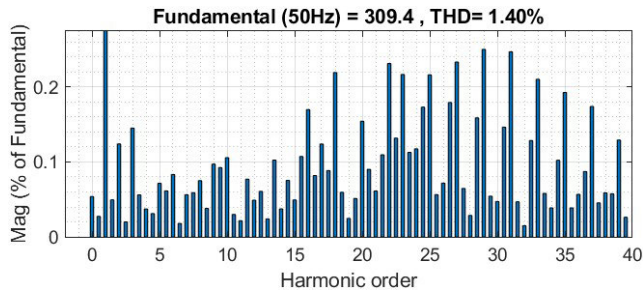


FIGURE 26. Three-phase load voltage FFT analysis under PI controller when the exact system parameters are unknown.

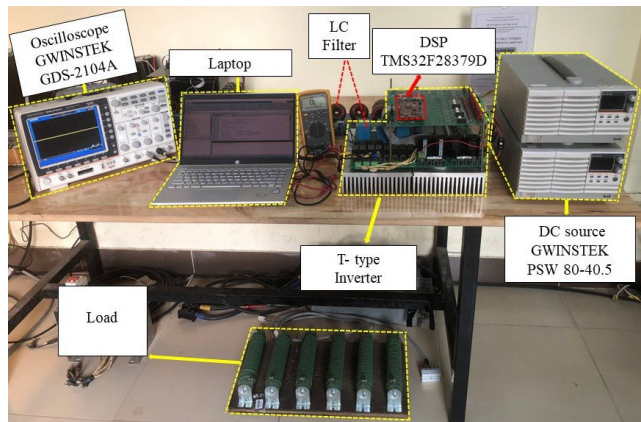


FIGURE 27. The experiment environment.

By applying the LMI to solve the stability of Eq. (45) to obtain the gains of state observer.

C. FTSMC FOR THE TPTL T-TYPE INVERTER

To archive the FT of the reaching phase, the SMC surface is proposed as follows:

$$s = e + \lambda \int_0^t e(\tau) d\tau \quad (46)$$

where λ is positively defined, $e = X_r - \hat{X}$, X_r is reference input.

Differentiating for Eq. (46) yields

$$\dot{s} = \dot{e} + \lambda \cdot e \quad (47)$$

With $\dot{s} = 0$, combined with the Eq. (42) lead to

$$\dot{X}_r = A\hat{X} + Bu + E\hat{l} - LC(X - \hat{X}) - \lambda e \quad (48)$$

$$\Rightarrow u_{eq} = (B^T B)^{-1} B^T [\dot{X}_r - A\hat{X} - E\hat{l} - LC(X - \hat{X}) + \lambda e] \quad (49)$$

To get the FT stability, the switching value is designed as

$$u_{swj} = \rho_{1j} |s_j|^{\frac{c_{1j}}{d_{1j}}} \text{sign}(s_j) + \rho_{2j} |s_j|^{\frac{c_{2j}}{d_{2j}}} \text{sign}(s_j) \quad (50)$$

where ρ_{1j} and ρ_{2j} are the switching gains, which are used such the force value of the sliding mode control. c_{1j} , c_{2j} , d_{1j} and d_{2j} are the real number, these value is used such as the operation order of the reaching law These mentions values need to be positively defined.

D. STABILITY OF THE PROPOSED METHODS

Lyapunov candidate is selected as follows:

$$V(s_j, \tilde{d}_j) = \frac{1}{2} s_j^2 + \frac{1}{2} \tilde{l}_j^2 \quad (51)$$

where s_j is the surface of sliding mode for d and q axes off voltage and current loops. Differentiating of both sides of Eq. (51) yields

$$\dot{V}(s_j, \tilde{d}_j) = s_j \dot{s}_j + \tilde{l}_j \dot{\tilde{l}}_j \quad (52)$$

Combining Eqs. (47), (50), and (51), the system in the first time without disturbance effect.

$$\dot{V}(s_j) = -s_j^T \cdot \rho_{1j} |s_j|^{\frac{c_{1j}}{d_{1j}}} \text{sign}(s_j) + \rho_{2j} |s_j|^{\frac{c_{2j}}{d_{2j}}} \text{sign}(s_j) < 0 \quad (53)$$

By using lemma 1, the settling time for the reaching phase is then the FT stability. The general settling time can be represented as follows:

$$T_j < T_{\max j} = \frac{1}{\rho_{1j}} \frac{d_{1j}}{c_{1j} - d_{1j}} + \frac{1}{\rho_{2j}} \frac{d_{2j}}{c_{2j} - d_{2j}} \quad (54)$$

The system with fully embedded DO will leads the settling time is as follows.

$$T_j < T_{\max_all} = \frac{1}{\rho_{1j}} \frac{d_{1j}}{c_{1j} - d_{1j}} + \frac{1}{\rho_{2j}} \frac{d_{2j}}{c_{2j} - d_{2j}} + \frac{\tilde{l}(0)}{\kappa} \quad (55)$$

The structure of the proposed control system is shown in Figure 3.

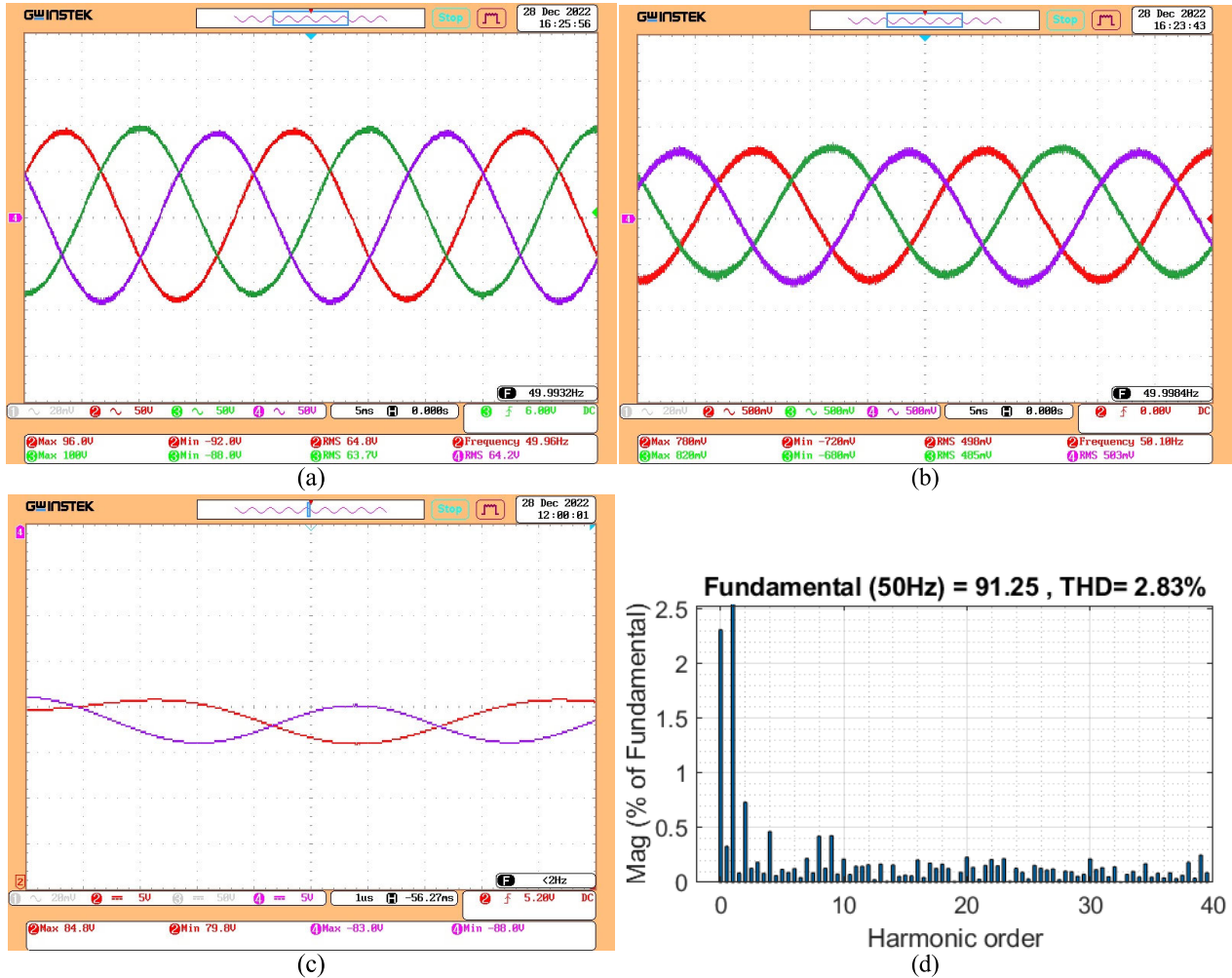


FIGURE 28. Experimental steady-state responses of (v_{La}, v_{Lb}, v_{Lc}) , (i_{La}, i_{Lb}, i_{Lc}) , (V_{c1}, V_{c2}) and THD under linear load.

Remark 8: The control parameters selection are the main effected factors of the control output performances. Herein, the LMI was used to obtain the gains of state observer.

The details of the proposed control algorithms for the TPTL T-type inverter is represented in the above Figure 3.

V. SIMULATION AND EXPERIMENTAL RESULTS

A. SIMULATION RESULTS

Simulation is implemented by using MATLAB software. The simulation parameters are given in Table 2.

First, the parameters of the components of the T-type inverter for the simulation study are listed in the Table 2 below.

The control gains for the simulation study are selected such as in the Table 3 below.

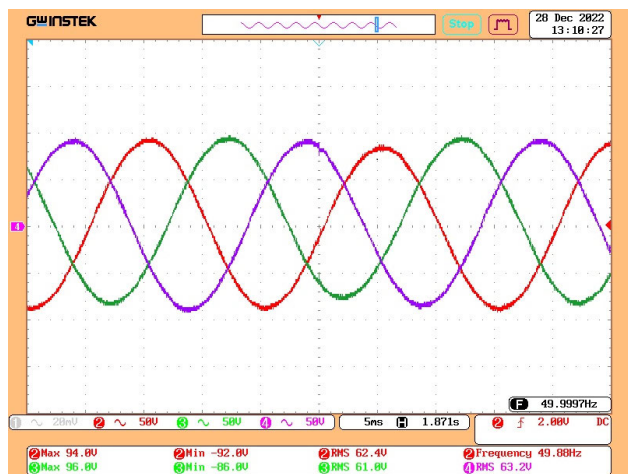
Fig. 4 shows the simulated steady-state responses of load voltage (v_{La}, v_{Lb}, v_{Lc}) , line current (i_{La}, i_{Lb}, i_{Lc}) , line-to-line voltage between phase a and phase b (v_{ab}) , and capacitor voltage (V_{c1}, V_{c2}) under a 9.68 (Ω) resistive load. In Fig. 4 (a), line-to-line voltage v_{ab} has the form of 5 levels, the same as the theory. Fig. 4 (c) shows that the neutral point voltage balancing is only 4.5V (about 0.9% of V_{DC}).

The FFT analysis of load voltage is shown in Fig. 5.

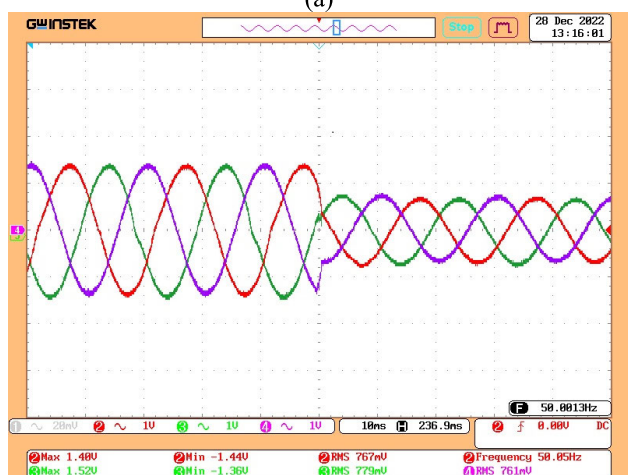
To show the superior of the sliding mode control, the phase plane of each given output are shown in Figure 7. There are the aims to show the reduced chattering phenomenon of used sliding mode controller.

The THD of the load voltage of the proposed controller is 0.44% ($<5\%$, according to IEEE 519-2014 standard). Fig. 8 shows the dynamic responses of load voltage, load current, capacitor voltage (V_{c1}, V_{c2}) for an abrupt change in the load resistance from 9.68 Ω to 5.808 Ω . As shown in Figs. 8 (a) and (b), the load voltage and load current exhibit very fast response to this load change so as to track their references. The voltage value on the load always follows the set value (220V RMS).

The capacitor voltage V_{c1} and V_{c2} are always balanced during the process, as shown in Fig. 8 (c). Figs. 10 and 12 showed the simulation results under the conditions of unbalanced load, there are two-phase load were used together with nonlinear load. Fig. 10 shows system response with unbalanced load, where the load current is unbalanced but the load voltage is still balanced and THD is 0.6%, which is shown in the Fig. 14. In the case of nonlinear load in Figs. 12



(a)



(b)

FIGURE 29. Experimental steady-state responses of (v_{La} , v_{Lb} , v_{Lc}) and (i_{La} , i_{Lb} , i_{Lc}) under load changes.

and 15, the load current is nonsinusoidal, however the load voltage is sinusoidal and THD is 1.17%.

Fig. 16 shows simulation results with the assumption that the exact system parameters are not unknown. The variations were used are as follows: $L_a = 90\%$, $L_b = L$ and $L_c = 110\%$, L , with L in Table 2). The load voltage and load current are still balanced and THD is 0.46% in Fig 18. Figs 6, 9, 11, 13 and 17 show the estimated and measured of the signals like d-axis voltage or current, which show that the SOB is working well. Figs. 4 to 18 show the simulation results of proposed controller under the conditions of balanced load, unbalanced load, load change, nonlinear load, and unknown system parameters. All of cases give sinusoidal voltage, three-phase balance, THD < 5%, the capacitor voltage V_{c1} and V_{c2} are always balanced. It proves that the proposed controller always works well with any kind of load or disturbance. To demonstrate the effectiveness of the proposed controller, a comparison is made with a PI controller. The outputs of the PI controller are shown in the Figures 19-26 below. The PI gains were selected by experience. The PI controller cannot reject

TABLE 4. Compare the proposed controller and PI controller.

Case	Proposed controller		PI controller	
	THD	Capacitor voltage	THD	Capacitor voltage
Linear load	0.44%	Balancing	0.61%	Balancing
Unbalanced load	0.60%	Balancing	>5%	Unbalancing
Nonlinear load	1.17%	Balancing	22.11%	Unbalancing
System parameters are not known exactly	0.46%	Balancing	1.4%	Balancing
Load changes	Fast dynamic response		Slow dynamic response	

the variation of inner and outer factors such as the uncertainty and disturbance due to the reason of that the PI is linear controller of error signal, which is the courses of the amplify the disturbance.

Figs. 19 to 26 show the simulation results under PI controller. The PI controller parameters for the voltage and current loop are selected as follows: $K_{pv} = 0.056$, $K_{iv} = 80$, $K_{pc} = 14$, $K_{ic} = 100000$. Figs. 19 and 20 show capacitor voltage (V_{c1} , V_{c2}), load voltage and current, and THD. The voltage difference between V_{c1} and V_{c2} is up to 8 V and THD is 0.61%, these values are much higher than the proposed controller use case. The dynamic responses of load voltage, load current under PI controller is shown in Figs. 20 and 21. Obviously, response speed of the proposed controller is many times faster than that of the PI controller. In particular, the PI controller gives bad control quality when the load is unbalanced, or the load is nonlinear. The system loses control when the load is unbalanced in Fig. 22. When the load is non-linear, THD is up to 22.11% such as in the Figs. 23 and 24. This value exceeds the allowable threshold in IEEE 519-2014 standard. The THD value of the output voltage when using PI controller is also affected if the system parameters are not known exactly. The unknown variations were used such as follows: $L_a = 90\%$, $L_b = L$, and $L_c = 110\%$, L , with L in Table 2 Then, THD is 1.4 % as in Fig. 26 while using proposed controller is only 0.46% as in Fig. 18. The comparison results between the proposed controller and PI controller are shown in Table 4. From the comparison results, the proposed controller is superior to the PI controller in all aspects.

B. EXPERIMENTAL RESULTS

The theory and test simulation results have been given in the above sections. The parameters of the components of the T-type inverter are listed in the Table 5 below.

The reason of difference between simulation and experiment is that the simulation is ideal and unlimited source of

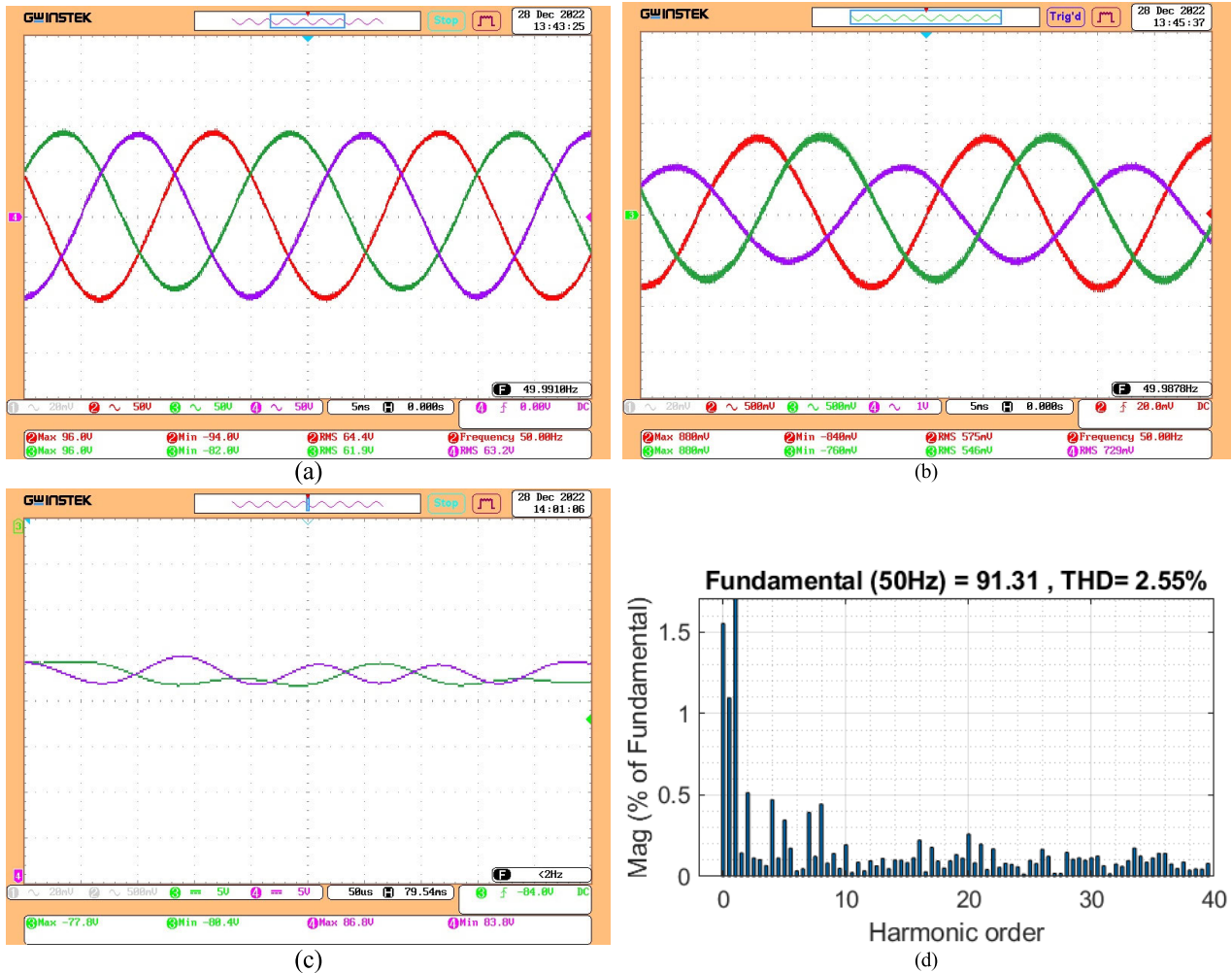


FIGURE 30. Experimental steady-state responses of (v_{La}, v_{Lb}, v_{Lc}) , (i_{La}, i_{Lb}, i_{Lc}) , (V_{c1}, V_{c2}) and THD under unbalanced load.

TABLE 5. Experimental parameters.

Parameters	Value
DC bus voltage	168V
Output voltage	112V/50Hz
Switching frequency	10kHz
LC filter	0.8mH/20μF
DC-link capacitor	940μF
Load	64Ω

devices. The experimental study is given based on the real facilities and application. The experimental setup is shown in Figure 27 below.

In the experiment, the devices are all displayed in the Figure 27. Where the system uses card F28379D, a TPTL T-type inverter, LC filter, R load and two DC power sup-

ply GWINSTEK PSW 80-40.5, which was used as the primary/secondary to obtain the large scale of supplied voltage source. To show the output voltage, the GW INSTEK GDS-2104A Digital Oscilloscopes (100Mhz, 4 CH, 2Gsa/s) was used. The Code Composer Studio with the version 12.2.0 was employed to implement the control algorithm. The computer with properties of Window 10, system type is 64bit, RAM 20GB, and core(TM) i5-8265U was used to write code for the microprocessor. The prototype of the experiment is shown in Fig. 27. Experimental scenarios are the same as simulation, where the balanced load, unbalanced load, load changes, nonlinear load or system parameters are not exactly known are all same with it in the simulation study. The experimental study results are shown below. Fig. 28 shows the experimental results under conditions of balanced load and load changes. In Fig. 28, both load voltage and load current are sinusoidal. The voltage value always follows the set value as 92V. The capacitor voltage V_{c1} and V_{c2} always balanced, and the maximum deviation is only about 4V. The .CSV file of the results is used to analyze THD on MATLAB/Simulink, THD is only 2.83%, which is shown in Fig. 28(d).

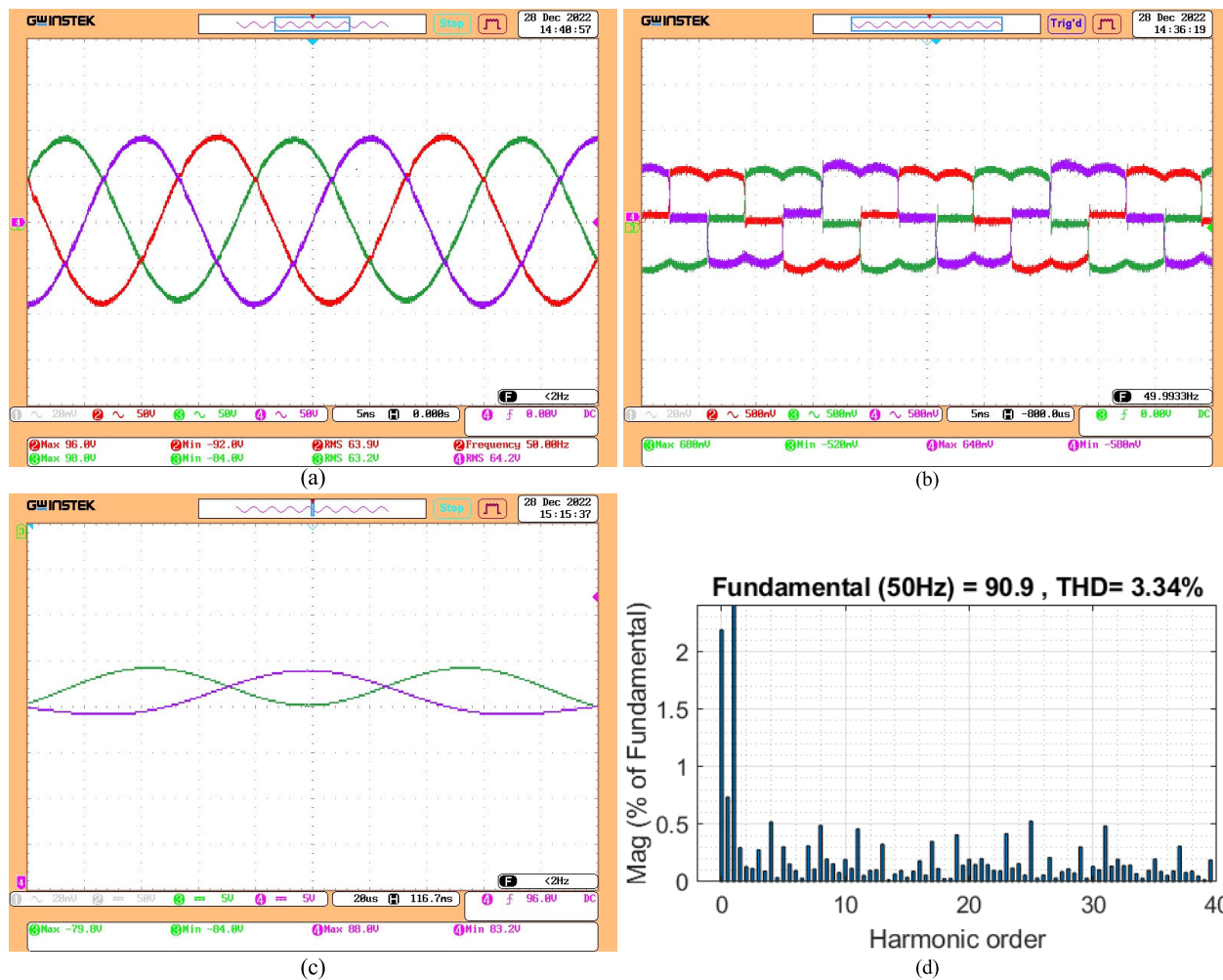


FIGURE 31. Experimental steady-state responses of (v_{La}, v_{Lb}, v_{Lc}) , (i_{La}, i_{Lb}, i_{Lc}) , (v_{C1}, v_{C2}) and THD under nonlinear load.

The dynamic response of the system when the load changes from 32Ω to 64Ω is shown in Fig. 29. The load currents exhibit a very fast response to this load change to track their references. The load voltages always follow the set value.

In Fig. 30, the results under an unbalanced load of two phases as 32Ω and the other phase 64Ω is shown. Same as the simulation results, the load current is unbalanced but the load voltage is still balanced and THD is 2.55% in Fig. 30(d).

True to theory and simulation, the experimental system under the proposed controller completely gives good results with cases of nonlinear load (Fig. 31) or unknown system parameters in Fig. 32. Under nonlinear load, THD is 3.34% in Fig. 31(d) and when unknown system parameters, THD is 3.03% in Fig. 32. Figs. 28 to 32 shows the feasibility of the controller when applied to a real-time system. The load voltages always are sinusoidal, and the frequency reaches 50Hz, as designed. It should be noted that the voltage value has a small error due to the use of deadtime or the error of the measuring device. The load current is measured by a current

sensor with an external resistance, so the magnitude value will be exponentially proportional. THD value is always less than 5%.

VI. CONCLUSION

This paper proposed a novel DOB for estimating the unwanted uncertain values and disturbances of the TPTL T-type inverter. The proposed DOB provided the finite-time convergent speed. The first derivative disturbance and fixed format requirement of the disturbance were completely removed. Furthermore, the FTSMC was provided to control the voltage and current of the T-type inverter, which helps the output of each subsystem converge to the predefined signal in a fixed time. The dependence of initial states was removed. To show the power and effectiveness of the proposed method, the stability of the proposed controller is proven mathematically. Furthermore, to support the validity of the proposed controller, the simulation and experiment has been carried out. The results demonstrated that the proposed controller give the good performances for output voltage such as fast

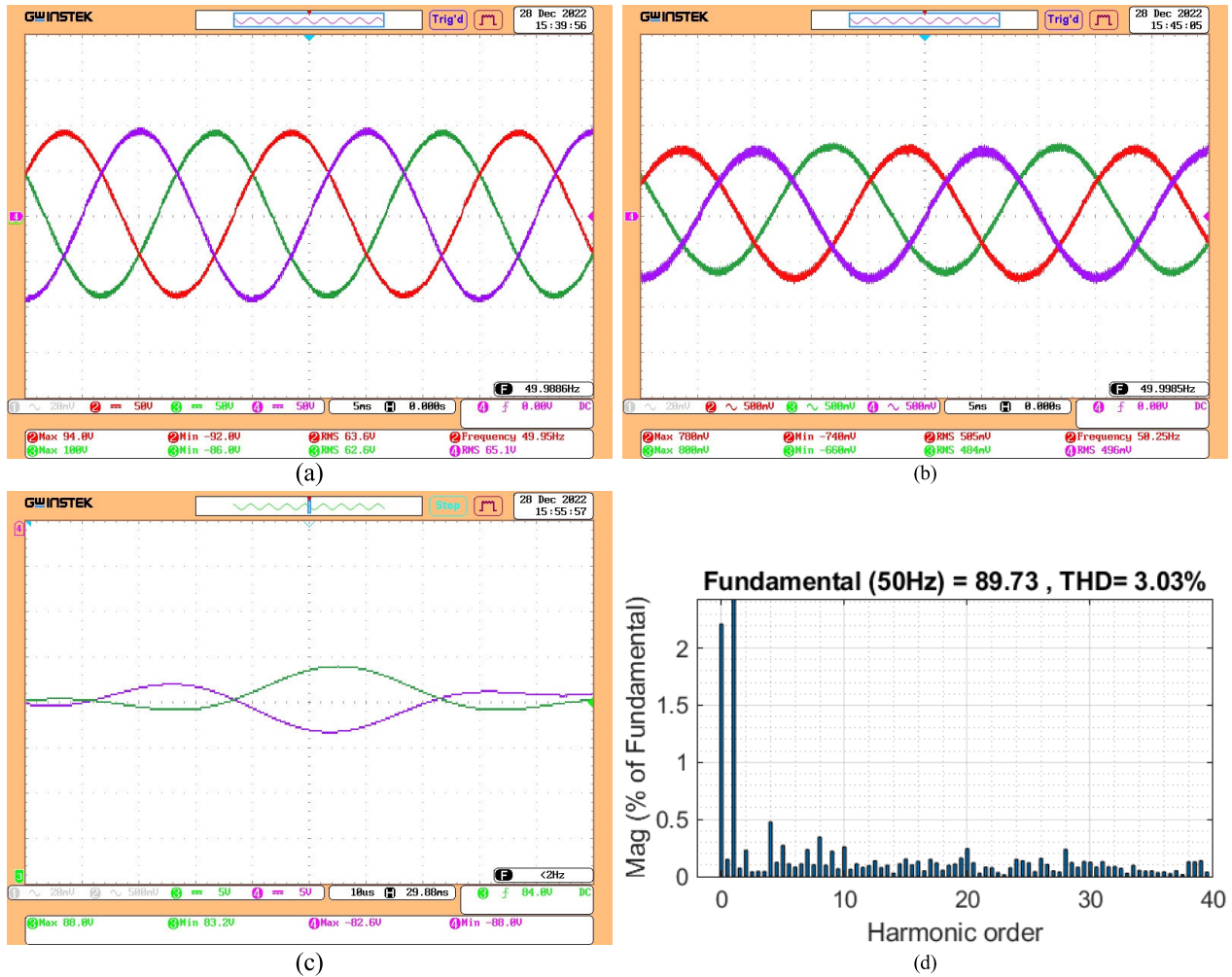


FIGURE 32. Experimental steady-state responses of (v_{La}, v_{Lb}, v_{Lc}) , (i_{La}, i_{Lb}, i_{Lc}) , (V_{C1}, V_{C2}) and THD when the system parameters are not known exactly.

dynamic, low THD under various conditions such as change of load, unbalanced load, nonlinear load, balanced load with the presence of system uncertainties, the capacitor voltages is always balanced.

REFERENCES

[1] B. Guo, F. Wang, and E. Aeloiza, "A novel three-phase current source rectifier with delta-type input connection to reduce the device conduction loss," *IEEE Trans. Power Electron.*, vol. 31, no. 2, pp. 1074–1084, Feb. 2016, doi: 10.1109/TPEL.2015.2420571.

[2] J. D. Barros, J. F. A. Silva, and É. G. A. Jesus, "Fast-predictive optimal control of NPC multilevel converters," *IEEE Trans. Ind. Electron.*, vol. 60, no. 2, pp. 619–627, Feb. 2013, doi: 10.1109/TIE.2012.2206352.

[3] A. H. Bhat, N. Langer, D. Sharma, and P. Agarwal, "Capacitor voltage balancing of a three-phase neutral-point clamped bi-directional rectifier using optimised switching sequences," *IET Power Electron.*, vol. 6, no. 6, pp. 1209–1219, 2013.

[4] Y. Yin, J. Liu, J. A. Sánchez, L. Wu, S. Vazquez, J. I. Leon, and L. G. Franquelo, "Observer-based adaptive sliding mode control of NPC converters: An RBF neural network approach," *IEEE Trans. Power Electron.*, vol. 34, no. 4, pp. 3831–3841, Apr. 2019, doi: 10.1109/TPEL.2018.2853093.

[5] C. Liu, F. Zhao, G. Cai, N. Huang, J. Wang, and M. Wang, "Novel individual voltage balancing control scheme for multilevel Cascade active-front-end rectifier," *IET Power Electron.*, vol. 7, no. 1, pp. 50–59, 2014.

[6] C. A. Teixeira, D. G. Holmes, and B. P. McGrath, "Single-phase semi-bridge five-level flying-capacitor rectifier," *IEEE Trans. Ind. Appl.*, vol. 49, no. 5, pp. 2158–2166, Sep/Oct. 2013, doi: 10.1109/TIA.2013.2258877.

[7] J. Lee and K. Lee, "An open-switch fault detection method and tolerance controls based on SVM in a grid-connected T-type rectifier with unity power factor," *IEEE Trans. Ind. Electron.*, vol. 61, no. 12, pp. 7092–7104, Dec. 2014, doi: 10.1109/TIE.2014.2316228.

[8] J.-I. Itoh, Y. Noge, and T. Adachi, "A novel five-level three-phase PWM rectifier with reduced switch count," *IEEE Trans. Power Electron.*, vol. 26, no. 8, pp. 2221–2228, Aug. 2011, doi: 10.1109/TPEL.2010.2090900.

[9] D. Mukherjee and D. Kastha, "A reduced switch hybrid multilevel unidirectional rectifier," *IEEE Trans. Power Electron.*, vol. 34, no. 3, pp. 2070–2081, Mar. 2019, doi: 10.1109/TPEL.2018.2837053.

[10] H. Cheng, J. Kong, P. Wang, and C. Wang, "Hybrid control scheme for three-phase multilevel unidirectional rectifier under unbalanced input voltages," *IEEE Access*, vol. 7, pp. 29989–30001, 2019, doi: 10.1109/ACCESS.2019.2897799.

[11] M. Lak, Y. Tsai, B. Chuang, T. Lee, and M. H. Moradi, "A hybrid method to eliminate leakage current and balance neutral point voltage for photo-voltaic three-level T-Type inverter," *IEEE Trans. Power Electron.*, vol. 36, no. 10, pp. 12070–12089, Oct. 2021, doi: 10.1109/TPEL.2021.3073471.

- [12] P. Roy and A. Banerjee, "A study on performance parameters of three-level T-type inverter based PMSM drives for electric vehicles applications," *Elect. Eng.*, early access, pp. 1–14, Mar. 2023.
- [13] V. Rathore, D. Kumar, and K. B. Yadav, "A 5-level T-type inverter fed six-phase induction motor drive for industrial applications," *Int. J. Electron.*, early access, pp. 1–21, Dec. 2023.
- [14] R. Phukan, X. Zhao, C. W. Chang, D. Dong, R. Burgos, M. Debbou, and P. Asfaux, "Characterization and mitigation of conducted emissions in a SiC based three-level T-type motor drive for aircraft propulsion," *IEEE Trans. Ind. Appl.*, vol. 59, no. 3, pp. 3400–3412, May/Jun. 2023.
- [15] F. Barrero-González, C. Roncero-Clemente, J. Gutiérrez-Escalona, M. I. Milanés-Montero, E. González-Romera, and E. Romero-Cadaval, "Three-level T-type quasi-Z source PV grid-tied inverter with active power filter functionality under distorted grid voltage," *IEEE Access*, vol. 10, pp. 44503–44516, 2022, doi: [10.1109/ACCESS.2022.3170098](https://doi.org/10.1109/ACCESS.2022.3170098).
- [16] N. Mayorga, C. Roncero-Clemente, A. M. Llor, and O. Husev, "A simple space vector modulation method with DC-link voltage balancing and reduced common-mode voltage strategy for a three-level T-type quasi-Z source inverter," *IEEE Access*, vol. 9, pp. 82747–82760, 2021, doi: [10.1109/ACCESS.2021.3087035](https://doi.org/10.1109/ACCESS.2021.3087035).
- [17] C. Roncero-Clemente, E. Romero-Cadaval, M. Ruiz-Cortés, and O. Husev, "Carrier level-shifted based control method for the PWM 3L-T-type qZS inverter with capacitor imbalance compensation," *IEEE Trans. Ind. Electron.*, vol. 65, no. 10, pp. 8297–8306, Oct. 2018, doi: [10.1109/TIE.2018.2814020](https://doi.org/10.1109/TIE.2018.2814020).
- [18] H. Kim, Y. Kwon, S. Chee, and S. Sul, "Analysis and compensation of inverter nonlinearity for three-level T-type inverters," *IEEE Trans. Power Electron.*, vol. 32, no. 6, pp. 4970–4980, Jun. 2017, doi: [10.1109/TPEL.2016.2607226](https://doi.org/10.1109/TPEL.2016.2607226).
- [19] W. Zhong, H. Wu, Z. Wu, C. Wei, T. Lou, and H. Zhao, "Control strategy of three-phase T-type three-level converter with reactive power compensation function," in *Proc. IEEE 5th Int. Elect. Energy Conf. (CIEEC)*, Nanjing, China, May 2022, pp. 2598–2603, doi: [10.1109/CIEEC54735.2022.9845819](https://doi.org/10.1109/CIEEC54735.2022.9845819).
- [20] S. Bayhan, H. Komurcugil, and I. S. Bayram, "Deadbeat control of a three-phase T-type inverter with output LC filter for UPS applications," in *Proc. IEEE 30th Int. Symp. Ind. Electron. (ISIE)*, Kyoto, Japan, Jun. 2021, pp. 1–6, doi: [10.1109/ISIE45552.2021.9576216](https://doi.org/10.1109/ISIE45552.2021.9576216).
- [21] P. Alemi, S.-Y. Jeong, and D.-C. Lee, "Active damping of LLCL filters using PR control for grid-connected three-level T-type converters," *J. Power Electron.*, vol. 15, no. 3, pp. 786–795, May 2015.
- [22] S. A. Khan, Y. Guo, and J. Zhu, "Model predictive observer based control for single-phase asymmetrical T-type AC/DC power converter," *IEEE Trans. Ind. Appl.*, vol. 55, no. 2, pp. 2033–2044, Mar. 2019.
- [23] D. O. Boillat, F. Krismer, and J. W. Kolar, "EMI filter volume minimization of a three-phase, three-level T-type PWM converter system," *IEEE Trans. Power Electron.*, vol. 32, no. 4, pp. 2473–2480, Apr. 2017.
- [24] K. Sun, X. Lin, Y. Li, Y. Gao, and L. Zhang, "Improved modulation mechanism of parallel-operated T-type three-level PWM rectifiers for neutral-point potential balancing and circulating current suppression," *IEEE Trans. Power Electron.*, vol. 33, no. 9, pp. 7466–7479, Sep. 2018.
- [25] J. Chen, C. Zhang, X. Xing, and A. Chen, "A fault-tolerant control strategy for T-type three-level rectifier with neutral point voltage balance and loss reduction," *IEEE Trans. Power Electron.*, vol. 35, no. 7, pp. 7492–7505, Jul. 2020, doi: [10.1109/TPEL.2019.2955600](https://doi.org/10.1109/TPEL.2019.2955600).
- [26] M. Kojima, K. Hirabayashi, Y. Kawabata, E. C. Ejiogu, and T. Kawabata, "Novel vector control system using deadbeat controlled PWM inverter with output LC filter," in *Proc. Conf. Rec. IEEE Ind. Appl. Conf. 37th IAS Annu. Meeting*, Pittsburgh, PA, USA, Oct. 2002, pp. 2102–2109, doi: [10.1109/IAS.2002.1043821](https://doi.org/10.1109/IAS.2002.1043821).
- [27] P. Mattavelli, "An improved deadbeat control for UPS using disturbance observers," *IEEE Trans. Ind. Electron.*, vol. 52, no. 1, pp. 206–212, Feb. 2005, doi: [10.1109/TIE.2004.837912](https://doi.org/10.1109/TIE.2004.837912).
- [28] P. Cortes, G. Ortiz, J. I. Yuz, J. Rodriguez, S. Vazquez, and L. G. Franquelo, "Model predictive control of an inverter with output LCLC filter for UPS applications," *IEEE Trans. Ind. Electron.*, vol. 56, no. 6, pp. 1875–1883, Jun. 2009, doi: [10.1109/TIE.2009.2015750](https://doi.org/10.1109/TIE.2009.2015750).
- [29] S. Jiang, D. Cao, Y. Li, J. Liu, and F. Z. Peng, "Low-THD, fast-transient, and cost-effective synchronous-frame repetitive controller for three-phase UPS inverters," *IEEE Trans. Power Electron.*, vol. 27, no. 6, pp. 2994–3005, Jun. 2012.
- [30] W.-H. Chen, D. J. Ballance, P. J. Gawthrop, and J. O'Reilly, "A nonlinear disturbance observer for robotic manipulators," *IEEE Trans. Ind. Electron.*, vol. 47, no. 4, pp. 932–938, Aug. 2000.
- [31] X. Wu, K. Xu, M. Lei, and X. He, "Disturbance-compensation-based continuous sliding mode control for overhead cranes with disturbances," *IEEE Trans. Autom. Sci. Eng.*, vol. 17, no. 4, pp. 2182–2189, Oct. 2020.
- [32] A. T. Nguyen, B. A. Basit, H. H. Choi, and J.-W. Jung, "Disturbance attenuation for surface-mounted PMSM drives using nonlinear disturbance observer-based sliding mode control," *IEEE Access*, vol. 8, pp. 86345–86356, 2020.
- [33] V. N. Giap, H. Vu, Q. D. Nguyen, and S. Huang, "Robust observer based on fixed-time sliding mode control of position/velocity for a T-S fuzzy MEMS gyroscope," *IEEE Access*, vol. 9, pp. 96390–96403, 2021, doi: [10.1109/ACCESS.2021.3095465](https://doi.org/10.1109/ACCESS.2021.3095465).
- [34] S. Hwang and H. S. Kim, "Extended disturbance observer-based integral sliding mode control for nonlinear system via T-S fuzzy model," *IEEE Access*, vol. 8, pp. 116090–116105, 2020.
- [35] V.-N. Giap, S.-C. Huang, Q. D. Nguyen, and T.-J. Su, "Robust control-based disturbance observer and optimal states feedback for T-S fuzzy systems," *J. Low Freq. Noise, Vib. Act. Control*, vol. 40, no. 3, pp. 1909–1925, 2021, doi: [10.1177/1461348420981181](https://doi.org/10.1177/1461348420981181).
- [36] V. N. Giap, Q. D. Nguyen, N. K. Trung, and S. C. Huang, "Time-varying disturbance observer based on sliding-mode observer and double phases fixed-time sliding mode control for a T-S fuzzy micro-electro-mechanical system gyroscope," *J. Vib. Control*, vol. 29, nos. 7–8, pp. 1927–1942, 2022, doi: [10.1177/10775463211073199](https://doi.org/10.1177/10775463211073199).
- [37] V. N. Giap, S. Huang, Q. D. Nguyen, and T. Su, "Disturbance observer-based linear matrix inequality for the synchronization of Takagi–Sugeno fuzzy chaotic systems," *IEEE Access*, vol. 8, pp. 225805–225821, 2020, doi: [10.1109/ACCESS.2020.3045416](https://doi.org/10.1109/ACCESS.2020.3045416).
- [38] S. Shi, J. Li, and Y. Fang, "Extended-state-observer-based chattering free sliding mode control for nonlinear systems with mismatched disturbance," *IEEE Access*, vol. 6, pp. 22952–22957, 2018, doi: [10.1109/ACCESS.2018.2828868](https://doi.org/10.1109/ACCESS.2018.2828868).
- [39] D.-T. Do, V.-T. Tran, M.-K. Nguyen, and S. M. Naik, "Fault tolerant control methods for three-level boost T-type inverter," *IEEE Trans. Ind. Electron.*, vol. 70, no. 6, pp. 5463–5473, Jun. 2023, doi: [10.1109/TIE.2022.3196341](https://doi.org/10.1109/TIE.2022.3196341).
- [40] W. Zhang and Y. He, "A simple open-circuit fault diagnosis method for grid-tied T-type three-level inverters with various power factors based on instantaneous current distortion," *IEEE J. Emerg. Sel. Topics Power Electron.*, vol. 11, no. 1, pp. 1071–1085, Feb. 2023, doi: [10.1109/JESTPE.2022.3194150](https://doi.org/10.1109/JESTPE.2022.3194150).
- [41] Z. Xing, Y. He, and W. Zhang, "An online multiple open-switch fault diagnosis method for T-type three-level inverters based on multimodal deep residual filter network," *IEEE Trans. Ind. Electron.*, vol. 70, no. 10, pp. 10669–10679, Oct. 2023, doi: [10.1109/TIE.2022.3222663](https://doi.org/10.1109/TIE.2022.3222663).
- [42] D. A. Tuan, P. Vu, and N. V. Lien, "Design and control of a three-phase T-type inverter using reverse-blocking IGBTs," *Eng., Technol. Appl. Sci. Res.*, vol. 11, no. 1, pp. 6614–6619, Feb. 2021.
- [43] Y. Tian, Y. Cai, and Y. Deng, "A fast nonsingular terminal sliding mode control method for nonlinear systems with fixed-time stability guarantees," *IEEE Access*, vol. 8, pp. 60444–60454, 2020, doi: [10.1109/ACCESS.2020.2980044](https://doi.org/10.1109/ACCESS.2020.2980044).



ANH TUAN DUONG received the B.S. and M.S. degrees from the Hanoi University of Science and Technology, Vietnam, in 2002 and 2007, respectively, all in control engineering and automation. Since 2003, he has been with the Hanoi University of Industry, where he is currently a Lecturer. His research interests include modeling and controlling of power electronics converters for applications, such as photovoltaic and electrical machine drives.



THANH LONG PHAM received the B.S. degree in control engineering and automation from the School of Electrical and Electronic Engineering, Hanoi University of Science and Technology, in 2023. He is currently a freelance researcher. His research interests include modeling and controlling of power electronics converters for applications, such as photovoltaic, wind systems, and electrical machine drives.



PHUONG VU received the B.S., M.S., and Ph.D. degrees from the Hanoi University of Science and Technology (HUST), Vietnam, in 2006, 2008, and 2014, respectively, all in control engineering and automation. He is currently a Lecturer with the Department of Automation, School of Electrical and Electronic Engineering (SEEE), HUST, where he is also an Associate Professor of control engineering and automation. His research interests include power electronics converters for applications, such as renewable energy, electric vehicle, and motor drives.

...



VAN NAM GIAP received the B.S. degree in control engineering and automation from the Hanoi University of Science and Technology, Hanoi, Vietnam, in 2015, the master's degree in electronic engineering from the National Kaohsiung University of Applied Sciences, Kaohsiung, Taiwan, in 2017, and the Ph.D. degree in mechanical engineering from the National Kaohsiung University of Science and Technology, Taiwan, in June 2021. He is currently with the Hanoi University of Science and Technology. His research interests include sliding mode control, disturbance and uncertainty estimation, fuzzy logic control, secure communication, magnetic bearing systems and its applications, and self-bearing motors.